The Nb-Ta-Zr-REE mineralisation of the Motzfeldt alkaline magmatic complex, south Greenland.

Liam Clark

A MASTERS THESIS in Economic Geology, Master of Science, submitted to University of Oulu

ABSTRACT

The Motzfeldt alkaline magmatic complex (MAMC) in southern Greenland is an interesting plutonic assemblage that may contain a valuable resource Nb-Ta-Zr-REE. It is a member of the set of alkaline intrusive rocks called the Gardar intrusions which occurred during a period of Proterozoic rifting (1,350-1,140 Ma). These includes also the prospective Ilímaussaq intrusion which is enriched in Rare Earth-elements. The relationship to this deposit, plus the period of magmatism make the MAMC a potential prospect to be explored.

At a regional scale, a geochemical dataset was used to determine the differences between three formations found in the MAMC. The normative mineralogy of the three formations show distinct variation but all three have a constant peralkalinity signature. This indicates that the three formations have a similar source composition and evolution. However, the oldest and middle formations underwent alteration that caused variation in their normative mineralogy. Elevated silica and trace element compositions related to the peralkaline rocks towards the edge of the MAMC indicates that mobilization of volatiles was achieved through the incorporation of country rock. Large scale circulation of fluids formed an 'outer shell' enriched in Nb-Ta-Zr-REE and SiO_2 particularly during the intrusion of the mid Motzfeldt Sø formation.

At a local scale, separate layers of an outcrop were sampled and analyzed to determine compositional variations between them. The samples were composed of syenites, microsyenites and pegmatites. A very late stage volatile rich fluid derived from the degassing of peralkaline microsyenites formed Nb-Zr-Ta-REE rich pegmatites at layer boundaries and caused fracturing at the microsyenite contacts. The host minerals for these elements, found in thin section of the pegmatites, include pyrochlore, zircon, thorite, eudialyte and bastnäsite.

The samples have also been compared to other known REE deposits. The pegmatite samples are characterized by a low LREE/HREE ratio and a relatively high TREE. However, the samples are not representative of the deposit as a whole. Further exploration needs to be done to assess the extent and regional continuity of the microsyenite sheets and associated pegmatites to fully appraise economic value.

ACKNOWLEDGEMENTS

I would like to thank Samuel Weatherley and the staff at GEUS for not only making my time in Copenhagen memorable but providing the data and samples for a most interesting project. This extends to Lotte Melchior Larsen for her historical data which made the examination of the regional dataset possible. I would also like to thank my supervisor Professor Holger Paulick for his patience and guidance though this process.

Contents

1. Introduction

Alkaline igneous rocks are of great interest as they are one of the main hosts of most igneous rare earth elements (REE) deposits. They are defined as rocks derived from small degrees of partial melting of ultramafic rocks Often they also contain an excess of alkali metals ($Na_2O + K_2O$) compared to SiO_2. In such melts, the alkalis cannot all be accommodated in feldspars alone and precipitate uncommon sodium- and potassium- bearing minerals (feldspathoids, alkali pyroxenes and amphiboles). These rocks are known to often contain excessive amounts of rare metals such as Li, Be, Nb, Ta, Zr, Th and rare earth elements (REE). They also can contain complexing volatile agents such as F and Cl making them of great interest. Typically, these rocks are related to the partial melting of an enriched mantle source rock in extensional settings (Chankhmouradian & Wall, 2012).

Alkali rocks in general range from mafic to felsic in composition. Volumetrically they only constitute about 1% of all igneous rocks at the earth surface but are particularly common in ocean islands and continental rifts (Walters & Lusty, 2011). Alkaline rocks have a significant geologic and economic significance due to the tendency towards containing high concentrations of trace elements. Bradshaw (1988) noted that the Motzfeldt alkaline magmatic complex (MAMC) in Greenland could be a significant host of increased concentrations of trace elements in certain peralkaline rocks of the ring complex. The excellently exposed, glacially scoured MAMC gives a unique opportunity to study a well preserved alkaline intrusion and associated mineralization.

The MAMC (1,310 ± 31 Ma (Blaxland, et al, 1978) is a cylindrical body roughly 15 x 20 km^2 which intruded into the Julianehåb batholith during a prolonged period of Proterozoic alkaline magmatism (1,350-1,140 Ma). It is associated with tectonic rifting in the central granite zone of the Ketilidian mobile belt in southern Greenland. It is part of the Gardar Province which consists of 12 major intrusive complexes intruded during an era of intense rifting of the supercontinent Laurentia, between 1,350-1,140 Ma (Bradshaw, 1988; Upton et al., 1996 and Garde et al., 1996). It is a multi-intrusion alkaline ring complex consisting of three main formations: Geologfjeld formation (GF), Motzfeldt Sø formation (MSF) and Flinks Dal Formation (FDF). It is dominated by syenites, nepheline syenites, syenogabbro and minor intrusives (Bradshaw, 1988; Tukiainen, 2014; MacDonald & Upton, 1993). Bradshaw (1988), Thomassen (1989) and Steenfelt (1991), estimate that there is a potential 600 x 10^6 tons of rock in the GF and the MSF that could host contents of up to 1320-1480 ppm Nb, 110-130 ppm Ta, 50-60 ppm U and 70-100 ppm Th. These estimates are based upon gamma-ray spectrometry and chip sample analysis.

Most of the previous work on the MAMC has been done in the context of regional geological studies of the many intrusive units of the Gardar Province (eg: Upton, 2013; Tukiainen, 2014; MacDonald & Upton, 1993; and Bradshaw, 1988). However, only a few studies have concentrated on the Nb-Ta-Zr-REE (NTZR) mineralization. These indicate a significant role of late stage peralkaline magmatism (McCreath, 2012; Bradshaw, 1988; Tukiainen, 2014 and Steenfelt, 1991, Thomassen, 1989). Bradshaw (1988) produced a comprehensive study of the regional geochemistry and petrogenesis of the MAMC and identified areas of interest including the Stoorelv valley to the north east and areas within the MSF. But there has been little work done to constrain the source, the mineralization, controlling factors and timing.

The rare earth elements (REE) are a group of 17 transition metals; the lanthanides (fifteen metallic chemical elements with atomic numbers from 57 to 71) plus scandium (Sc) and yttrium (Y). They are classified as specialty metals mainly used in the high-tech spectrum: batteries, new materials, catalysts, environmental protection, aerospace, and electronic information industries (Voncken, 2013, Chankhmouradian & Wall, 2012). They are of specific interest due to their increasing demand and a severe global market imbalance. Almost 97% of all REE mine production originates in China. Hence, the rest of the world relies heavily on Chinese exports. It is expected that, due to this ever-increasing market demand and supply imbalance, there will be REE shortages and price increases in the future (Brumme, 2014).

With increasing demand of REE and increasing pressure on Europe to find local sources, there has been a boom in interest in potential European REE deposits. This thesis presents bulk rock geochemical, and petrographic analysis of both regional and targeted samples of the MAMC. It aims to better define the different formations, rock types and understand the element partitioning between them. Specific attention is directed towards the mineralization of Nb-Ta-Zr-REE in the Stoorelv valley, with the aim to constrain the source, concentrations, the controlling factors and timing. Finally, this thesis will look at the MAMC as a potential new source of Nb-Ta-Zr-REE in the context of global and regional world resources.

2. Geological background

2.1 Regional geology and geochronology

The Motzfeldt alkaline magmatic complex (MAMC) is situated on the southern tip of Greenland lying 24 km to the east of the village of Narsarsuaq (Figure 1) and 100 km from the Atlantic coast. The MAMC is a spectacular, glacially eroded valley occurring north east of the agpaitic intrusive units of the Ilímaussaq intrusion (Tukiainen, 2014).

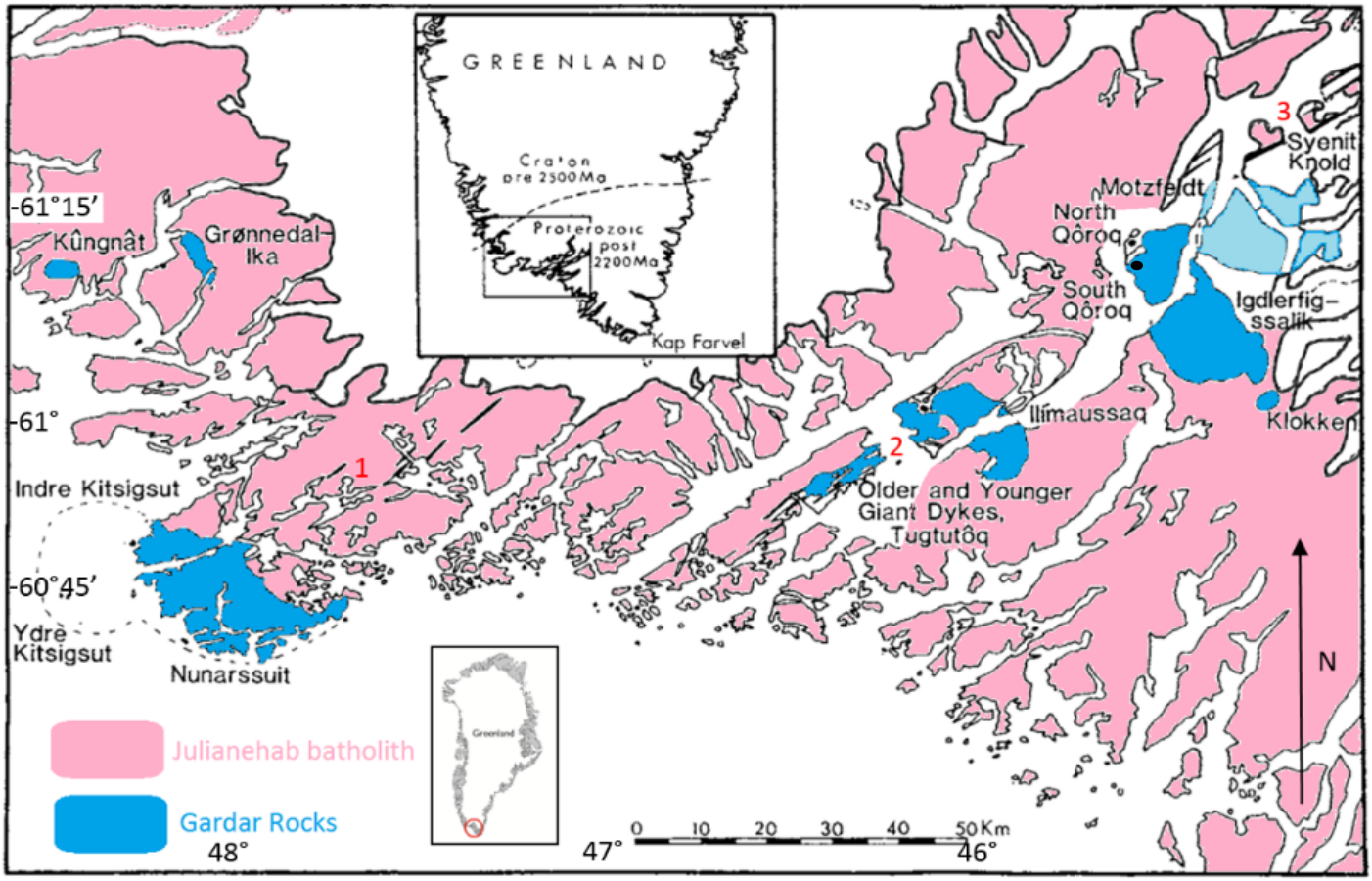

Figure 1 Geological sketch map of south Greenland. Showing the Gardar suite of rocks (blue) which intruded into the Julianehåb batholith (pink). Also noted are the other names of the Gardar rocks and the location of the MAMC in (light blue) where the main study area is located. Altered from Tukiainen, (2014) and Upton, et al., (1996). Also added are the location of the Tugtutoq-Ilimaussaq (2-3) and Nunarssuit-Isortoq (1) extensional lineaments from MacDonald & Upton, (1993). Age dating has placed the MAMC intruding concurrently with the western Grønnedal-Ika intrusion. The black dot indicates the village of Narsarsuaq.

The MAMC is one of the 12 major intrusive alkaline complexes comprising the Gardar intrusions (GI). These occurred in a cyclic nature corresponding to changing tensional stresses in the crust, which are structurally controlled along three major faulting lineaments seen in Figure 1 (MacDonald & Upton, 1993 and Bradshaw, 1988). The GI's intruded into the reworked Archaean terranes of the Eriksfjord formation; which consists of: quartzites, basalts trachytes and phonolites and the main I-type granitic Julianehåb formation (Bradshaw, 1988). Both of these formations make up the majority of the overlying Julianehåb batholith (Figure 1).

Geochronologically, the GI's can be split into two main episodes of magmatism: Early Gardar, from 1,310-1,250 Ma and Late Gardar is at 1,230-1,130 (Rb-Sr) and 1,180-1,140 Ma derived U-Pb age determinations, (Upton, 2013 and Upton, 1978). Blaxland, et al. (1978), studied Sr and Rb isotope ratios over the entire MAMC taking samples from the GF, MSF, and FDF. They noted significant scatter in the isochron data possibly representing contamination. However, consensus is that the MAMC occurred during the Early Gardar spanning 1,280–1,255 Ma (eg: Blaxland et al. 1978; Upton and Emeleus 1987; Upton et al. 2003 and Upton, 2013). At this time, undersaturated magma was being produced at both ends of the Gardar province since the undersaturated Grønnedal-Ika intrusion (*Figure 1*) 150 km west is of similar age. McCreath (2012) also studied the age relationships of the MSF and the alteration that occurred within the MSF. He showed that the magmatic emplacement of the MSF occurred at 1,273 ± 6 Ma but there is evidence of secondary polyphase fluid interaction within this formation causing alteration in the pyrochlore which gives an isochron age of 1,267 ± 6 Ma. This alteration is a product of an alkaline hydrothermal phase which occurred shortly after the magmatic phase.

The GI's were emplaced by a combination of block sloping, ring fracture and partial dyke formation along two main tensional stress regimes active along E-W and NE-SW liniments (marked by 1,2 and 3 in Figure 1). These were inferred from the orientation of faults and dykes. The melt was drawn from mantle depths during rifting and dilation along inherent mechanical weaknesses of the Julianehåb batholith (Upton, 1978; Upton el al., 2003; McCreath, 2012). Most of the GI magmatism is associated with a Proterozoic rift system which preceded the Grenville (Sveconorwegian) orogenic activity (Upton, 1978). The variety of rock types is explained by differentiation of magmas from a parental alkali olivine basalt primary melt (Blaxland et al., 1978).

Upton (1978) has also suggested that the high concentrations of trace elements in Gardar rocks was linked to a mantle source which was enriched by volatile flux processes and further raised by fractionation of these magmas. Abundant anorthosite inclusions in some Gardar rocks indicate that substantial plagioclase crystal fractionation took place. High values for Al, Fe/Mg and (K+Na)/Ca ratios can be explained by clinopyroxene fractionation at depths between 15 to 60 km (Upton, 1974).

2.2 Geologic setting

The MAMC is roughly circular with a diameter of 20 km and consists of three major formations and other minor intrusives related to prolonged intraplate continental tectonic rifting (Figure 2). The general structure of the MAMC comprises concentric steeply-dipping consecutive intrusions from a central intrusive rifting focus. It represents the exhumed plutonic suite of rocks that would have underlain a continental alkali volcanic province (Gill, 2010). It is composed mainly of intrusive alkaline rocks (nepheline syenites and alkali syenites) and later intrusive units that range in composition from basic to evolved rocks (Emeleus and Harry, 1970; Jones, 1984 and Tukiainen, 1988).

The MAMC can be divided into three distinct formations representing three periods of magmatism inner youngest: FDF, middle: MSF and the oldest: GF, the development can be seen in Figure 2 and Figure 3. The youngest inner core: (FDF) is about 5 km in diameter (7a-9b Figure 2 and Figure 3) and is composed of various types of undersaturated nepheline syenites. The outer ring: (MSF, 4a-4b in Figure 2 and Figure 3) is composed of more oversaturated syenites and is generally more altered (Bradshaw, 1988; McCreath, 2012). Towards the outer edges of

this formation there is an abundance of pegmatites and peralkaline sheets indicating that the later melt was highly enriched in volatiles. Finally, the satellite 'outer ring' GF (1-3, Figure 2 and Figure 3) consists mostly of nepheline syenites and some later peralkaline microsyenites derived from the MSF.

The sub-horizontal peralkaline sheets could contain appreciable amounts of Nb-Ta-Zr-REE mineralization Bradshaw (1988). They are located mainly in the outer edges of the MSF where it is in contact with the GF and the host Julianehåb batholith. They appear to be late stage peralkaline microsyenites and altered syenites that lie conformably within the units. The frequency and thickness of these sheets increase towards the outer edges of the MSF with an associated increase in textural heterogeneity and degree of alteration (McCreath et al., 2012).

Within each of these units there are several sub divisions noted in Figure 2 and Figure 3. Numerous pegmatites, large (m scale) syenogabbro and larvikite giant-dykes and smaller intrusives of the Ring Dyke formation (5-6b Figure 2 and Figure 3) are located throughout the MAMC cross cutting MSF and GF boundaries. Based on these cross cutting relationships the Ring Dyke formation is inferred to have been intruded during the period between FDF and MSF (Bradshaw, 1988).

Glaciation has largely eroded away the overlying Eriksfjord formation exposing the core of the FDF, MSF and the GF. The MAMC is cut by faulting trending NE-SW and more substantially E-W which has offsets of ~800 m (image E in Figure 3) (McCreath et al., 2012). Recrystallized and metasomatically altered xenoliths derived from the Eriksfjord Formation and older basement are found in the FDF and MSF. These indicate that the Erikfjord formation (EF) was in prolonged contact with active magma and that the FDF and MSF intrusion could have reached high into the basement stratigraphy (Blaxland et al., 1978).

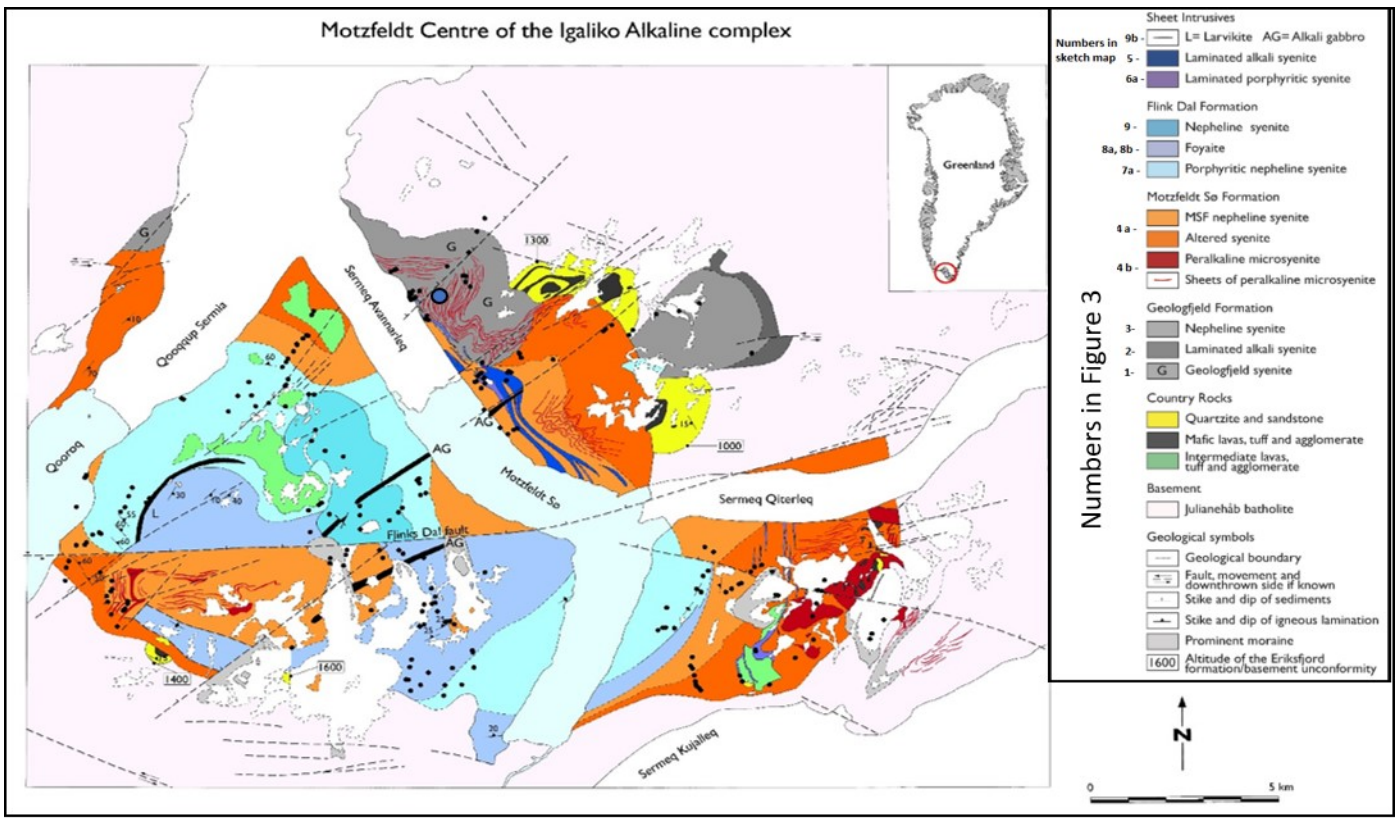

Figure 2 Detailed Geological map of Motzfeldt complex (Tukiainen, 2014) a more detailed geological map of image E in Figure 3. The blue dot indicates the location of the 2016 data collection outcrop while the black dots indicate the sample locations for the 'LML database 1984'.

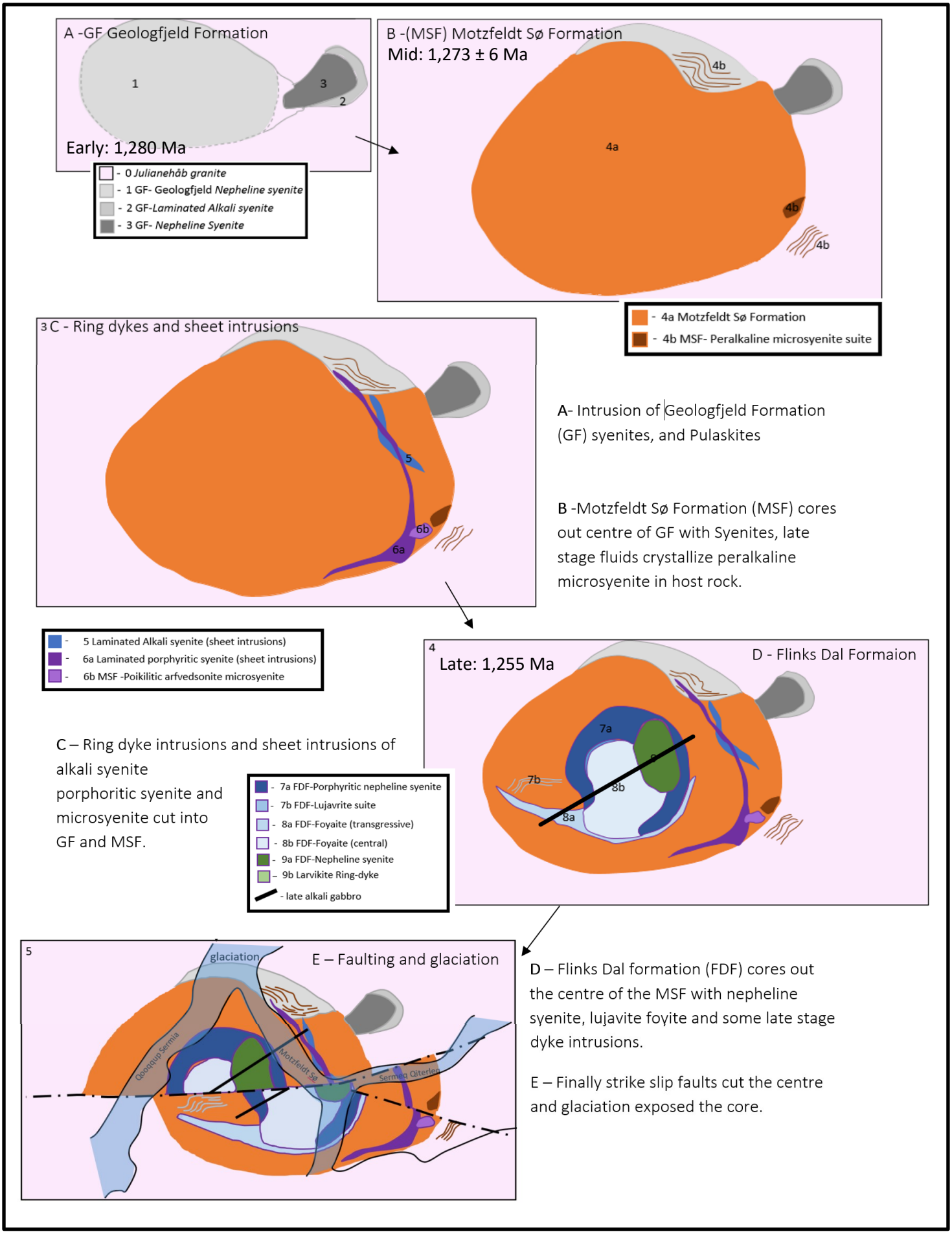

A- Intrusion of Geologfjeld Formation (GF) syenites, and Pulaskites

B -Motzfeldt Sø Formation (MSF) cores out centre of GF with Syenites, late stage fluids crystallize peralkaline microsyenite in host rock.

C – Ring dyke intrusions and sheet intrusions of alkali syenite porphoritic syenite and microsyenite cut into GF and MSF.

D – Flinks Dal formation (FDF) cores out the centre of the MSF with nepheline syenite, lujavite foyite and some late stage dyke intrusions.

E – Finally strike slip faults cut the centre and glaciation exposed the core.

Figure 3 Sketch map of the development of the MAMC adapted from (Bradshaw, 1988) showing the different intrusive bodies and the chronology of intrusions.

3. Lithological and mineralogical descriptions

Descriptions of the formations of the MAMC is presented based on previous work (Bradshaw, 1988; Steenfelt, 1991; Finch et al., 2001 and Upton et al., 2003).

3.1 Geologgfjeld formation (GF)

The formation of the MAMC began with the intrusion of the GF (1.300 Ma) (units 1, 2 and 3 in Figure 2 and Figure 3). It outcrops in the north and north-east of the MAMC in vast sheet like bodies. This period of magmatism intruded as three separate units. The first formed a central core of nepheline syenite followed by two smaller syenite satellite units towards the northeast of the central intrusion. It is composed of a coarse grained syenite called the GF syenite, and includes later microsyenites an associated pegmatites. It occurs mainly in large lenticular rafts aligned, long axis parallel to the contact. These rafts are surrounded by microsyenites and pegmatites. In some areas, later alteration associated with the younger MSF has discolored the GF syenites yielding a deep-brown to yellow appearance by forming secondary minerals of biotite and muscovite. Peralkaline sheets of microsyenites associated with the MSF intruded later into the GF.

The GF is formed of very coarse grained (1-3 cm) homogeneous syenites which are white in hand sample with dark green - black spots of amphibole and clinopyroxene. It is mainly undersaturated and composed predominantly of alkali feldspar and feldspathoids: nepheline or analcime ($NaAlSi_2O_6 \cdot H_2O$). Amphibole comprises up to 10% of the syenite and frequently includes Na-Ca-clinopyroxene and some olivine (Jones, 1984). The sheeted units are often separated by rounded pegmatitic segregations and microsyenites. The microsyenites are these are medium-fine grained (1-3mm) blue-grey in color and associated with pegmatites. Larger units of microsyenites often have a fractured contact filled with pegmatites. The pegmatites are often found between the contacts of the microsyenites and the GF syenite and occur in cm scale units (Weatherley, 2016). The unit is described as displaying cumulus textures common also in the other Southern Greenland intrusions and indicative of in situ fractional crystallization (Bradshaw, 1988).

3.2 Motzfeldt Sø formation (MSF)

The second stage of intrusive units, the MSF, lasted from 1.273 Ma to 1.267 Ma. The MSF (units 4a and 4b in Figure 2 and Figure 3), occupies the main syenite body of the MAMC. It originally intruded into the center of the GF coring out the older unit and making it a satellite unit to the north-east. This formation typically exists as a coarse grained syenite with alkali feldspar (up to 60%), nepheline (varying from 0-25%) and Na-Ca pyroxenes and amphiboles (15%). Amphibole is normally arfvedsonite and can range from 20-60 wt%. Other minor minerals are fluorite, zircon, aenigmatite and pyrochlore. The syenite shows high amounts of pervasive alteration which has caused the breakdown of primary amphibole minerals to Fe-Ti oxides and secondary micas suggesting that hydrothermal activity was intimately associated with this unit (Bradshaw, 1988).

The outer edges of the MSF, representing contact zones with the roof and sides of the magma chamber, show distinct changes in crystallization. Near contacts the MSF has lamination orientation of the crystals. In the more altered samples quartz crystals occur and these samples are generally much more feldspathic. Such sheets host vast complexes

of pegmatic patches. Genetically related to these altered syenites are the peralkaline microsyenites of the MSF occurring in sheets that are conformably arranged with the Julianehåb batholith contact. Both of these MSF units have been associated with Zr-Nb-Th-U-Be-REE enrichment. However the peralkaline pegmatite rich outer and upper margins of the MSF are typically sites of this mineralization. Bradshaw (1988 & 1986) noted that there were many accessory minerals in these sheets including: eudialyte, zircon, bastnäsite and pyrochlore.

3.3 Flinks Dal Formation (FDF)

The final intrusive unit, the FDF (units 7a-9b in Figure 2 and Figure 3), occurred at 1.250 Ma and represents the innermost and youngest formation of the MAMC. It intruded mainly into the core of the older MSF and formed a central unit. It is comprised of several coarse-grained pale intrusive nepheline syenites that are slightly less evolved than the other formations. It is dominated by a core of mainly foyaite with 3-5 mm phenocrysts of alkali feldspar, nepheline and clinopyroxene and some rare olivine. Accessory minerals include sodalite, analcite, apatite, Fe- oxides and biotite. Accessory låvenite and rinkite have been noted throughout the formation (Jones, 1984). The largest areas of the FDF have steeply outward sloping contacts. The FDF contains many different textures but cumulus textures dominate. This formation is thought to be a relatively 'fresh' version of the MSF and GF with very little alteration and mineralization noted (Bradshaw, 1988).

4. Materials and methods

The present study is based on 275 regional samples collected by Lotte Melchior Larsen in 1984 named the 'LML database 1984'. This is supplemented by field data and 14 samples collected by Samuel Weatherley, Geological Survey of Denmark and Greenland, Copenhagen in the summer of 2016 focusing on the peralkaline microsyenites and pegmatites within the Stoorelv valley of the GF (figure 2).

Data given in appendix 1 and appendix 2 represents the bulk rock compositions of rock samples taken from the regional and local dataset respectively. For bulk rock geochemistry analysis of the local dataset, the original samples (~500g) were first cut into smaller hand samples weighing >100g each. From this roughly 200g of the original sample were crushed using a Mn steel jaw crusher into a coarse gravel (1-2mm). Then 60-100g of this gravel was removed and ground using a tungsten carbide ring mill into a fine power. Grinding usually took 4-5 minutes and between each sample appropriate cleaning of all equipment was done to prevent contamination. From this 10-20g of ground powder was sent to Bureau Veritas Minerals in Canada for analysis. The number of analyses made using different analytical methods is listed in appendix 2 and the methods used in Table 1.

The elements analyzed include major and trace elements including REE. Higher upper detection limits were used for Nb, Ta, major oxides, C, S and fluorine due to the importance in this study. For detecting trace elements (including REE and fluorine) inductively coupled plasma mass spectrometry (ICP-MS) was used. The detection limits are listed in appendix 1. For complete digestion, the sample powders were mixed with $LiBO_2/Li_2B_4O_7$ flux. This was then fused to a glass bead which was subsequently dissolved in ACS grade nitric acid. This method is especially effective for the most refractory and resistive mineral phases.

Major elements were analyzed using Whole Rock Lithium Fusion ICP Finish (appendix 1 shows detection limits) from the same solutions as generated for the trace element analysis. The loss on ignition (LOI) was determined by heating samples to 1000ºC for two hours to remove volitiles and measure the weight loss.

The total carbon and sulfur was determined by the LECO method: after weighing the material, it is heated and combusted in the presence of pure oxygen. During the process, carbon and sulfur are oxidized and the resulting CO_2 and SO_2 emissions are measured.

The LML database 1984 samples were analyzed using X-ray fluorescence spectrometry for major and trace element analysis. The FeO in the samples of the 1984 data were determined by titration.

Analytical methods		
Bureau Veritas Code	Method	Samples
LF100	ICP-MS for REE + trace elements	14
LF100	REEPKG higher upper detection limits for Nb, Ta	14
LF300	ICP-AES for major oxides	14
TC003	(C & S) (Leco method)	14
GC841	(ICP-MS for fluorine)	14
N/A	X-ray fluorescence spectrometry (major and trace elements)	275

Table 1 List of analytical methods used, the number of samples sent and where appropriate the Bureau Veritas Code

4.1 CIPW Norms and rock classification

For both sets of samples approximation of the mineral modes was calculated from the chemical analysis using CIPW norm (Cross, et al., 1902, calculation rules given by Kelsey, 1965). The major oxides and some other elements (SiO_2, TiO_2, Al_2O_3, Fe_2O_3, FeO, MnO, MgO, CaO, Na_2O, K_2O, P_2O5, CO_2, SO_3, S, F, and Cl) are entered in their oxide wt% plus some important elements (Sr, Ba, Ni, Cr, and Zr) in ppm and this can give an approximation of the modal mineral assemblage.

This calculation is an approximation and many assumptions must be made. This means that there are many areas where errors could occur. The calculations assume the magma is anhydrous thus minerals such as biotite or hornblende are not permitted. Other assumptions include ignoring minor solid solution elements and that all Fe/Mg ratios of all ferromagnesian minerals are the same (Rollinson, 1993). Normally this calculation is used for fine grained and glassy igneous rocks and rocks that have the same geochemistry but different grain size. However, this technique is useful in this case as the petrographic data for the LML 1984 rock samples are not available. Hence, the geochemistry can help classify these rocks by producing a normative mineralogy. These normative mineral abundances can be used in the Streckeisen classification diagram (Figure 4) which charts the abundances of four minerals: quartz (Q), alkali feldspars (A), plagioclase feldspars (P), and feldspathoids (F). From this diagram a rock name/ classification for plutonic rocks can be assigned to that sample based on its geochemical composition.

Another use of this diagram is to indicate magmatic compositions. The two halves of the diagram can represent two crystallization pathways. The upper half of the diagram could represent rocks that have formed from oversaturated melt and contain quartz, K-feldspar, and plagioclase. While the lower half of the diagram could contain rocks that have formed from undersaturated melt containing Feldspathoids, K-feldspar, and Plagioclase. This is reasonable as the degree of silica saturation will dictate the mineralogy of the crystalizing rock (Gill, 2010) e.g. with a silica undersaturated melt it will tend during cooling towards precipitating nepheline whereas a silica saturated melt will tend towards precipitating quartz. Thus, the placement of the rocks on this diagram represent the crystallization pathway the melt has taken. On the other hand, the placement of the sample could also represent contamination from external sources increasing the silica content and forcing the normative mineralogy into the upper half of the diagram.

Finally, the peralkalinity index is used in this thesis to determine the degree of differentiation of the melt. The peralkalinity index $(Na_2O)_{mol} + (K_2O)_{mol} / (Al_2O_3)_{mol}$ reflects the degree of magmatic differentiation and can somewhat explain the geochemical and mineralogical features (Le Bas, 1986). The petrogenesis of peralkaline rocks is often attributed to protracted fractional crystallization from a parental magma or a two-step process of low degree partial melting and low pressure fractional crystallization. Important boundary conditions under which magmatic differentiation occurs include temperature, crystal-melt equilibrium and volatile content.

5. Results - Regional data set

5.1 Regional scale major element systematics

The geochemical data set for the LML 1984 samples was accompanied by field rock descriptions which divided the samples into 13 different rock types (see the key of Figure 7). According to these descriptions the three formations appeared to be dominated by nepheline syenites, with the FDF described as a more porphyritic nepheline syenite. However, based on the normative mineralogy derived from CIPW calculations a different characterization emerges (Figure 4). The three formations have slightly different normative mineralogy and occupy distinct, but overlapping, spaces on the diagram. Overall, the three formations describe the MAMC in terms of its changing chemical composition over time from the oldest GF to the youngest FDF.

The oldest GF occupies the center of the diagram highlighted in green ranging from a silica poor foid-bearing monzonite to more silica rich quartz monzonite (Figure 4). In contrast the youngest FDF represents a much more silica under-saturated group dominated by foid-bearing monzonite to monzosyenite. The mid MSF (blue) has an intermediate composition with a varied pattern overlapping both the GF and the FDF from foid- rich to quartz dominated.

This changing geochemical composition is also apparent in the varying silica and total alkali content (Figure 5). Figure 5 shows the three formations plotted on a TAS (total alkali silica) diagram and shows the variation of SiO_2 and $Na_2O + K_2O$ (total alkalis). As the MAMC developed there is a reduction in the silica content and an increase in total

alkalis. The GF and MSF both have comparatively enriched SiO_2 content and a larger range of values (72%, to 49%). In contrast the youngest FDF has lower silica content (max: 57%, to 44%) grouping around 57% SiO_2.

Additionally, there is also a general trend of increasing total alkali as the MAMC developed. The GF has Na_2O + K_2O grouping around 12.5% and is not very variable. The MSF on the other hand has a very variable geochemical signature, the total alkali content groups similarly to the GF however there is higher variation within the dataset with upper and lower boundaries of 16% and 7% total alkali respectively. The youngest formation (FDF) groups around 15% Na_2O + K_2O with comparatively little variation. There is a lot of overlap between the three formations. However, the general trend of increasing Na_2O + K_2O and decreasing SiO_2 as the MAMC developed has been highlighted on figure 5 with a black arrow outlining the changing geochemistry with time.

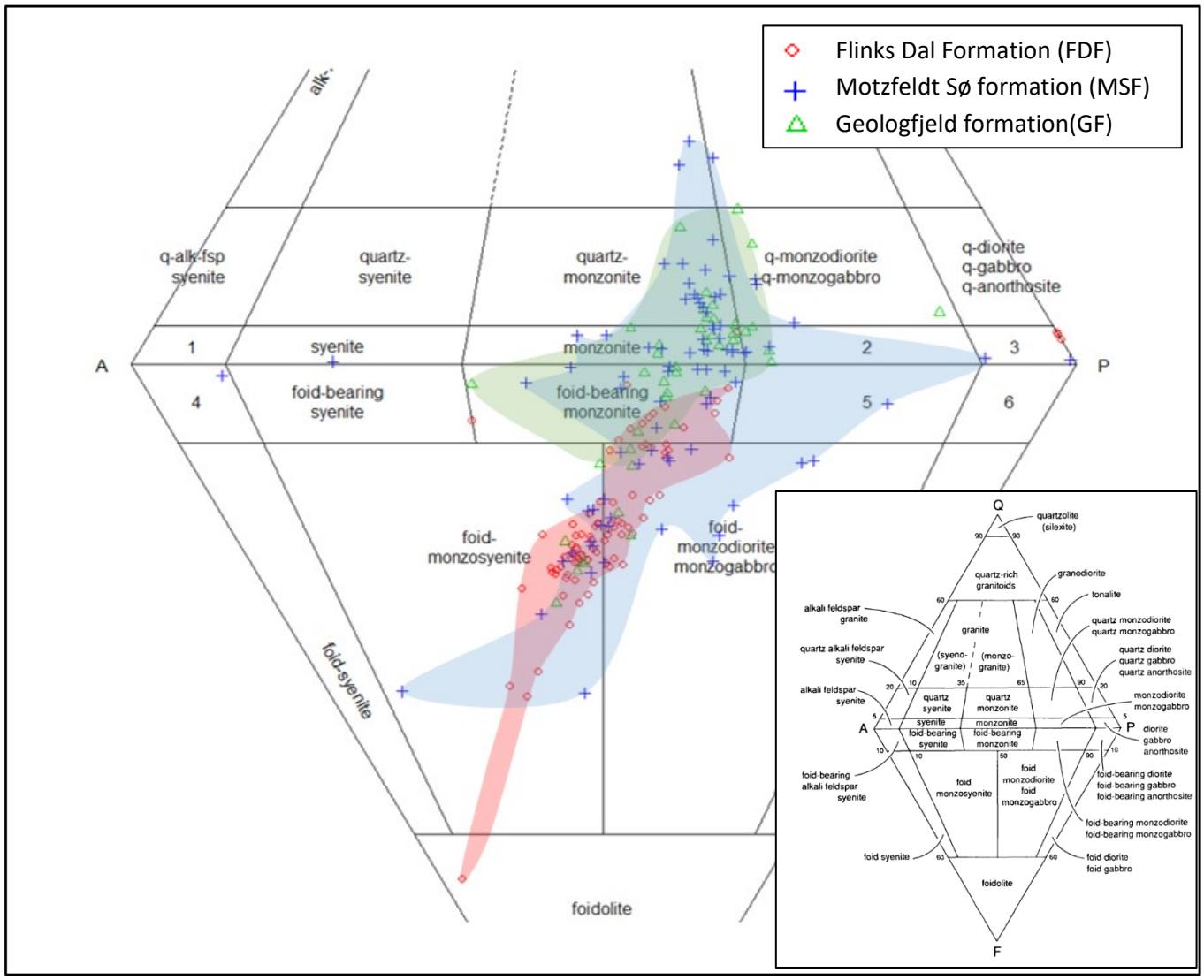

Figure 4 QAPF diagram (Streckeisen, 1974) showing the three main formations in the MAMC Green: Geologfjeld formation (GF); Blue: Motzfeldt Sø formation (MSF) and Red: Flinks Dal Formation (FDF). Overlay indicates the geochemical zones the three units occupy. GF occupies a central zone ranging from foid-bearing monzonite to quartz monzonite. The MSF has a much more varied pattern covering both zones from foid rich to quartz bearing. The FDF represents a much more silica under-saturated unit determined by foid monzosyenite, monzodiorite and monzogabbro. Insert: classification and nomenclature of the plutonic igneous rocks according to their felsic modal concentrations when mafic mineral content is less than 90%. Q, Quartz; A, alkali feldspar; P, Plagioclase; F, feldspahoid (foid) (Streckeisen, 1974)

The Na_2O:K_2O:Al_2O_3 molar proportions has been plotted in figure 6Figure for comparison with the trends observed in Figures 4 and 5. Unlike the TAS diagram the degree of magmatic differentiation is not distinguishable between the formations (therefore age) as all three formations significantly overlap, grouping at the peralkaline-metaluminous boundary and do not show an evolution trend with age. In summary, the samples have a distinct geochemical variation with age, evolving in terms of SiO_2 and total alkali content while the peralkalinity degree of differentiation does not appear vary significantly between the three formations.

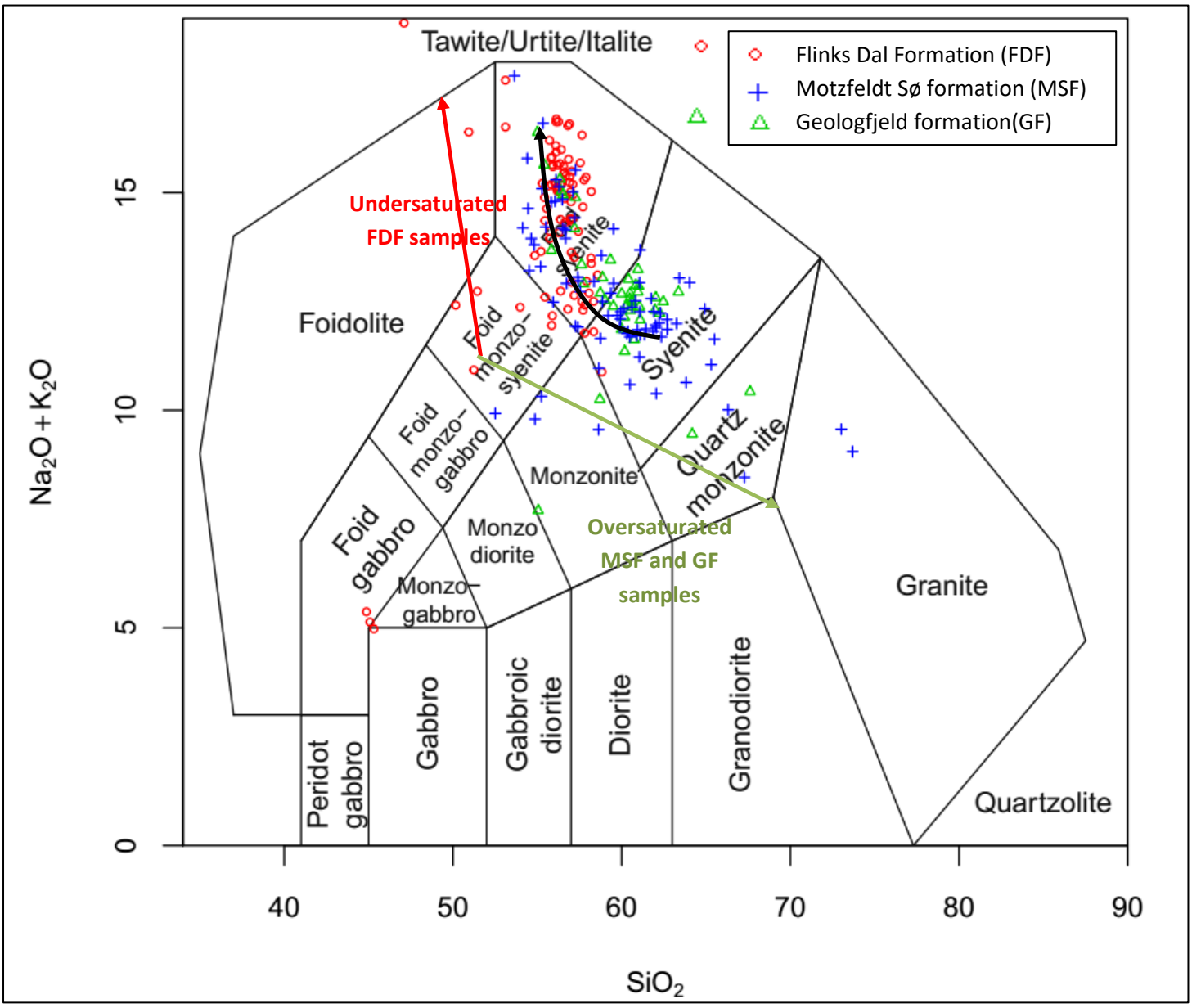

Figure 5 TAS (total alkali silica) diagram showing the three main formations in the MAMC Green: Geologfjeld formation (GF); Blue: Motzfeldt Sø formation (MSF) and Red: Flinks Dal Formation (FDF). Overlay indicates the groupings of the datasets into undersaturated high alkali and oversaturated low alkali. With the three formations intruded at different ages separated between these two groups. The black arrow shows the evolution of the geochemistry of the samples in the MAMC from the older GF and MSF to the younger FDF.

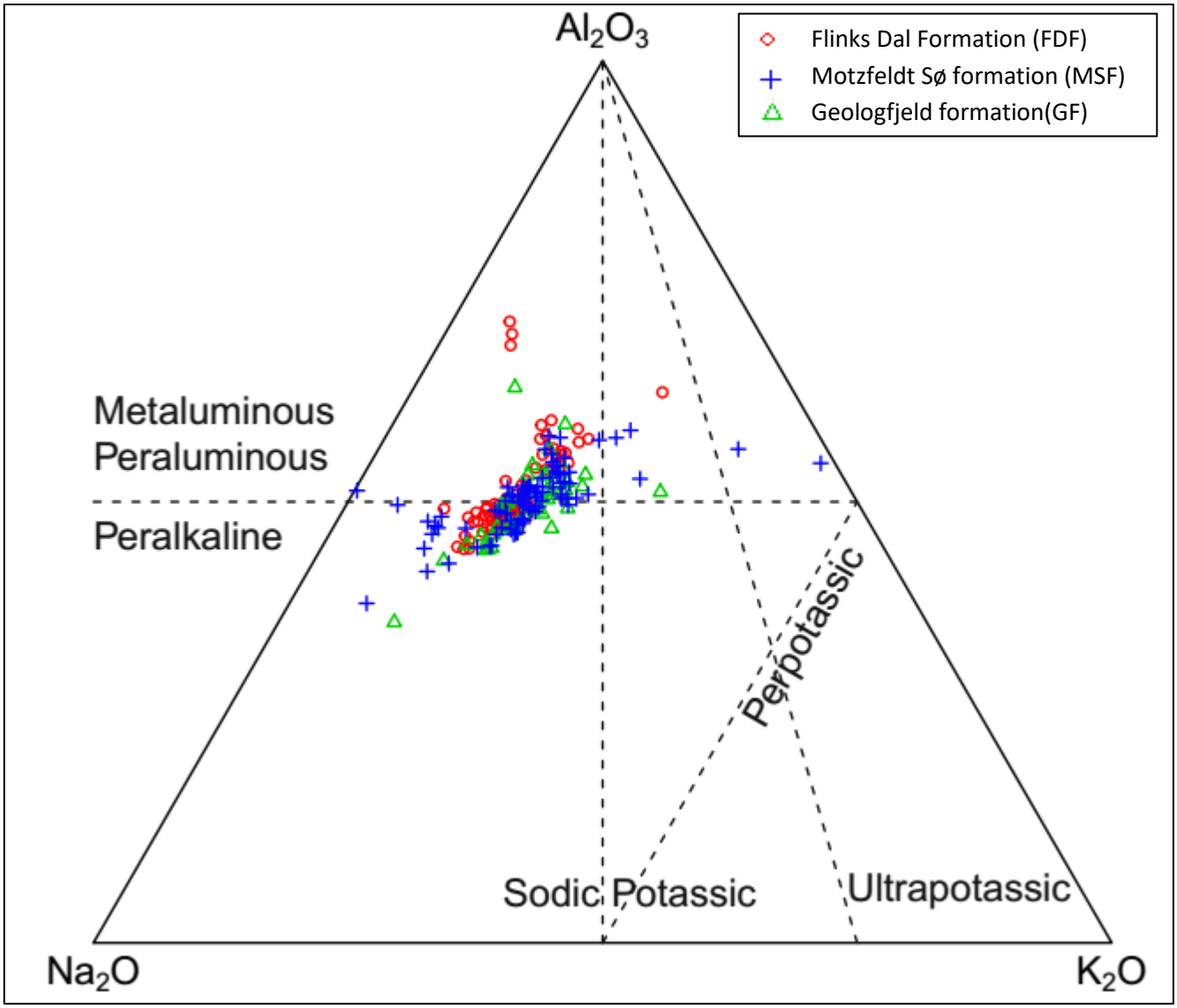

Figure 6 Molar Al_2O_3, Na_2O and K_2O plot on a ternary plot showing the three main formations in the MAMC Green: Geologgfjeld formation (GF); Blue: Motzfeldt Sø formation (MSF) and Red: Flinks Dal Formation (FDF). Peralkalinity is the ratio of $(Na_2O)_{mol}$+ $(K_2O)_{mol}$:($Al2O3)_{mol}$ and is indicative of the degree of differentiation the source magma has undergone. It is represented here in the lower left of the ternary diagram. The formations do not appear to be separated by their peralkalinity indicating similar degrees of differentiation over all three formations and at all stages of the MAMCs magmatic activity. Most samples are enriched in soda (Na_2O) rather than potash (K_2O) lying in the sodic series of rocks.

5.2 Regional scale trace element systematics

Trace elements in the MAMC show distinct variation between the different formations. Overall, the older GF and MSF have samples with the highest concentrations of Nb, Zr, Ta, La, Ce, Nd, Y, Pb, Th, Sc, Cr, Cu and Zn than the younger FDF. While individually the oldest GF has samples with the highest concentrations of Sc, the MSF has samples with the highest concentrations of Ce, Nd, La, Y, Nb, Zr and Ta. The youngest FDF in general has samples with higher concentrations of Rb, Sr, Ba, Cl, S, V and Ni compared to the other formations. The concentrations of key elements Nb, Ta, Zr and REE (NTZR), separated by formation and rock type according to field notes, are shown in figure 7 and illustrate this distinction.

In general, the concentrations of these elements correlate broadly positively with the peralkalinity index, ($Na_2O_{(MOL)} + K_2O_{(MOL)}$) / $Al_2O_{3\,(MOL)}$), i.e. the more peralkaline samples have a distinctly higher concentration of these key elements. This relationship is seen in figure 7. However more importantly, the higher concentration of these elements are found in samples of the MSF and the GF highlighted in Figure 7.

Figure 7 is split into three parts, A-H shows the NTZR concentration for the regional samples split by formation and rock type against modal qtz and modal ne wt%. There is no correlation between this modal mineralogy and the NTZR mineralization. Both modal qtz and modal ne wt% samples having mineralized and non-mineralized samples. The MSF and GF have a many more samples that are have higher wt% of modal qtz, while the FDF has a higher modal ne wt% signature. The main modal ne wt% rock type is porphyritic nepheline syenite (red) while the rest of the samples have variable modal mineralogy. The most mineralized rock type is the Peralkaline Microsyenite samples straddling the nepheline-quartz normative boundary, a few pegmatites, altered syenites and nepheline syenites also are mineralized at this boundary. Mineralized samples lie between 20% quartz and 20% nepheline wt% with no real trend to the silica saturation and NTZR mineralization. The more nepheline normative samples are the FDF samples with the MSF and GF lying on the nepheline-quartz normative boundary. These two formations have the highest NTZR concentrations.

Figures 7, I-P plot the Rb/Sr ratio. This ratio is normally related to the redistribution of Rb and Sr due to late- to post-magmatic alteration but when plotted with this dataset it shows no correlation between increased alteration and increased NTZR mineralization. Indicating little to no to late- to post-magmatic alteration in these samples.

Figure 7 Q-X show the dataset plotted against the peralkalinity index. There is significant overlap in peralkalinity between all three formations, as seen in Figure 6 and when compared to increasing concentrations of (NTZR) the samples do not fully positively correlate with increasing peralkalinity as seen. The MSF like the GF has many NTZR enriched samples but not all are peralkaline. The samples from the FDF are not particularly peralkaline or contain elevated concentrations of NTZR. Higher concentrations of these elements lie at a peralkalinity index between 0.25-1.6 with the highest concentrations generally around a value of 1 especially in the REE. However as indicated by the red line there is an apparent threshold of peralkalinity 0.9 which when crossed there is greater potential for mineralization to occur.

Separating the samples by rock types (figure 7, right hand images) clearly shows that the concentrations of these elements are restricted to a specific rock type: ‘peralkaline microsyenites’, with some of the more peralkaline nepheline syenites also having much higher concentrations. These peralkaline microsyenites have higher concentrations are restricted to the MSF and the GF (figure 7) There is also one altered syenite in the MSF that has higher concentrations of REE but is not peralkaline. The highest concentration of REE in a sample lies in a peralkaline microsyenite from the GF. Additionally, some of the MSF nepheline syenites and microsyenites contain almost 1% Zr but are not peralkaline. The correlation of key elements, Nb, Zr, Ta and REE with time (MSF emplacement) and rock type (peralkaline microsyenite) may have some genetic link.

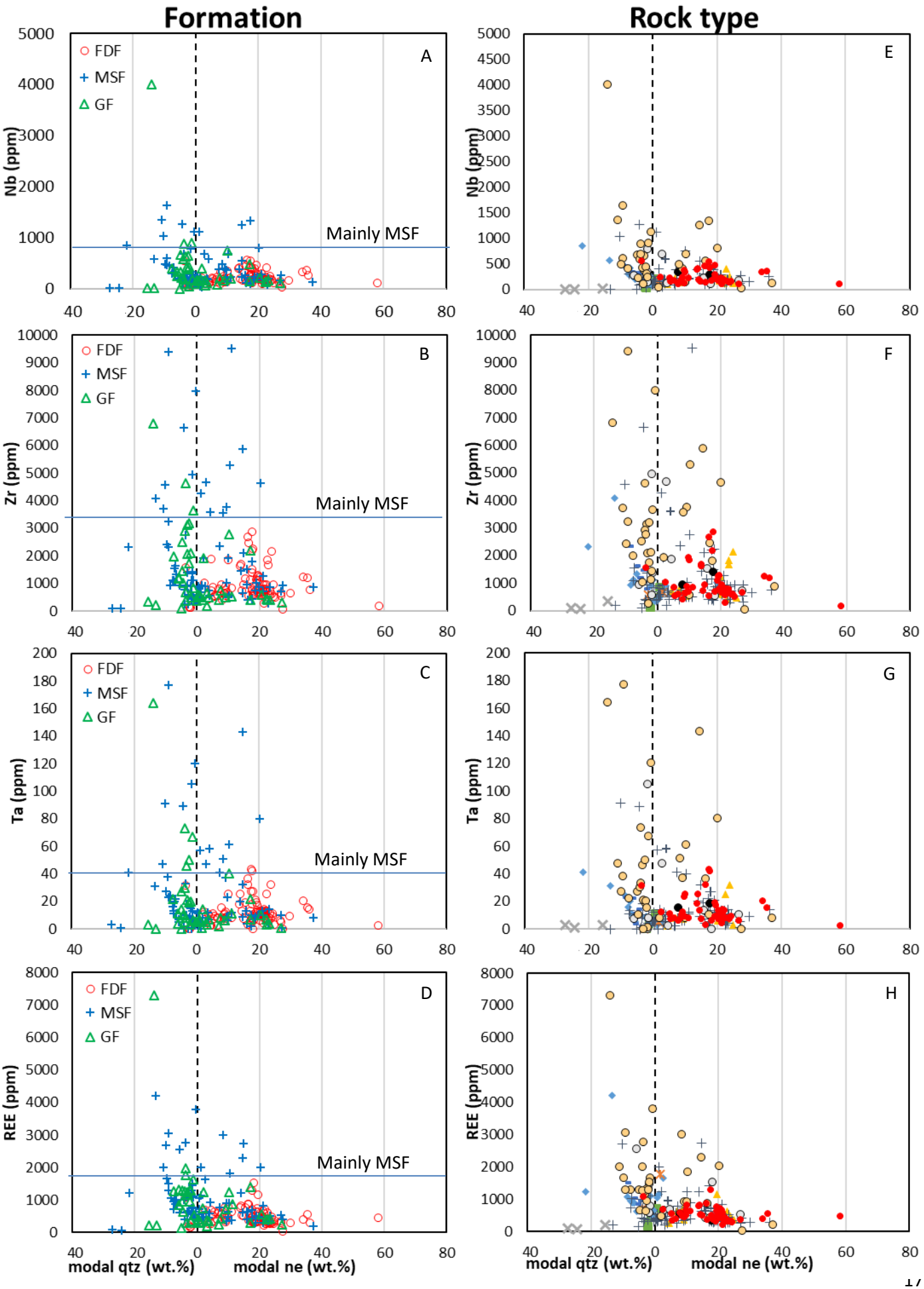
Formation
Rock type
A
B
C
D
E
F
G
H
FDF
MSF
GF
Mainly MSF
Nb (ppm)
Zr (ppm)
Ta (ppm)
REE (ppm)
modal qtz (wt.%)
modal ne (wt.%)

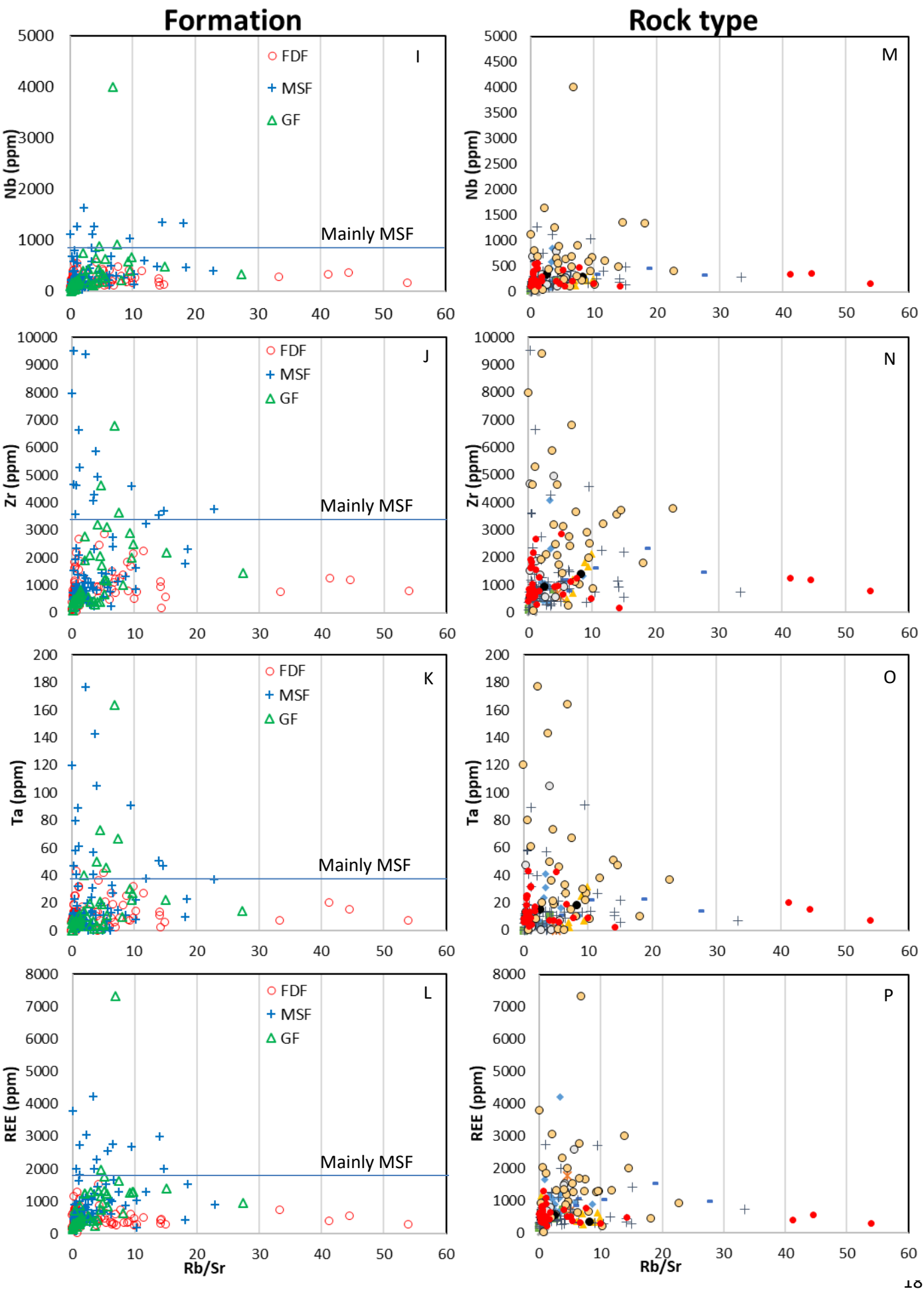
Formation
Rock type
I
M
J
N
K
O
L
P
FDF
MSF
GF
Mainly MSF
Nb (ppm)
Zr (ppm)
Ta (ppm)
REE (ppm)
Rb/Sr

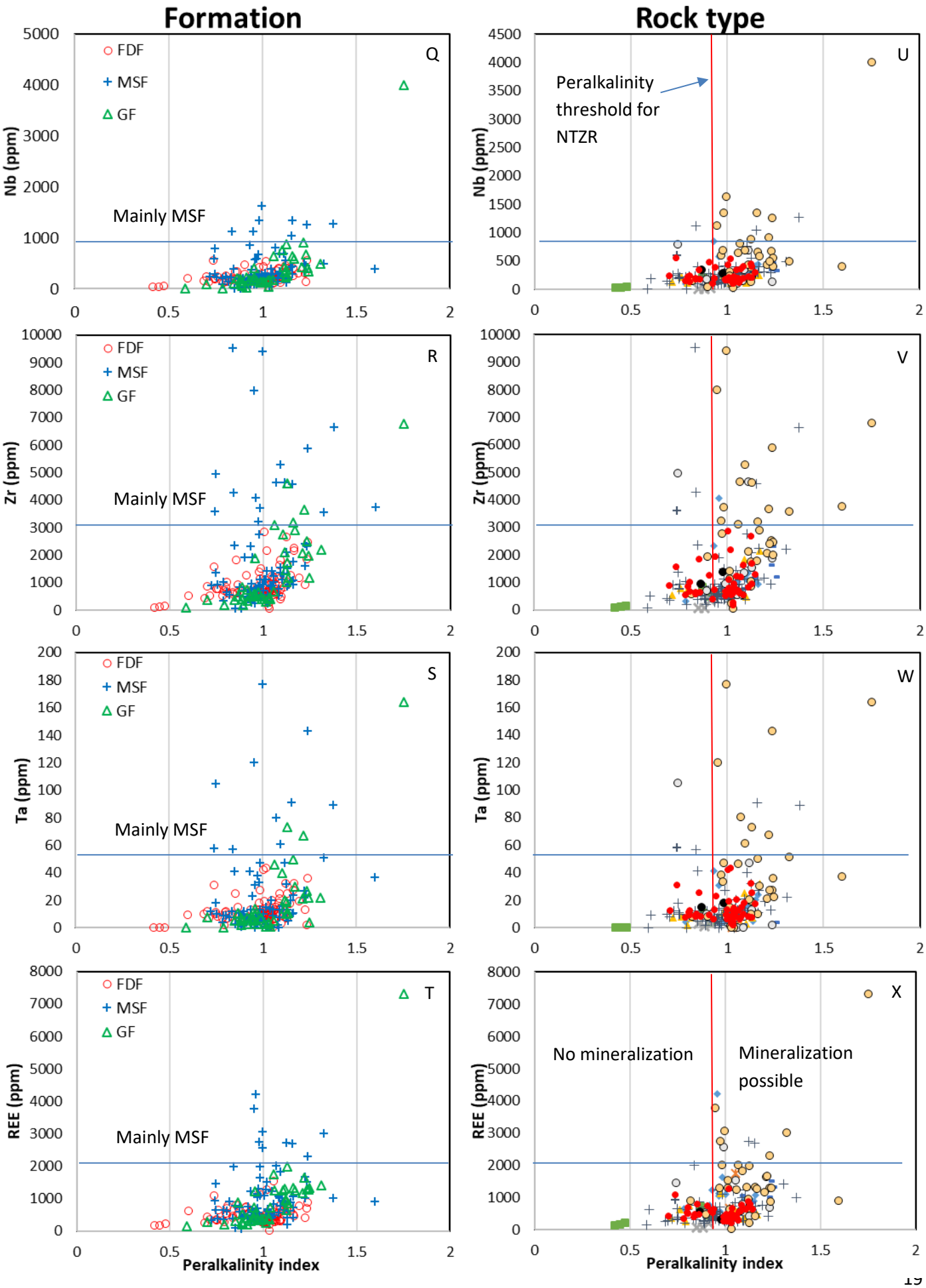
Formation
Rock type
FDF
MSF
GF
Q
U
R
V
S
W
T
X
Nb (ppm)
Zr (ppm)
Ta (ppm)
REE (ppm)
Mainly MSF
Peralkalinity threshold for NTZR
No mineralization
Mineralization possible
Peralkalinity index

Figure 7 (Previous pages) All regional samples plotted. Elements of interest in this study (Nb, Zr, Ta, and the REE) are plotted on the y axis in ppm against (image: A-H) The modal qtz (wt.%)/modal ne (wt.%), (image: I-P) the Rb/Sr ratio and (Image: Q-X)Peralkalinity index (Na2O) mol+ (K2O) mol/ (Al2O3) mol.

Images on the left hand side distinguish the samples based upon the formation from which they were derived: Green: Geologfjeld formation (GF); blue: Motzfeldt Sø formation (MSF) and Red: Flinks Dal Formation (FDF).

The right hand images distinguish the samples based upon the rock type which are directly taken from notes made in the field. The key is shown below:

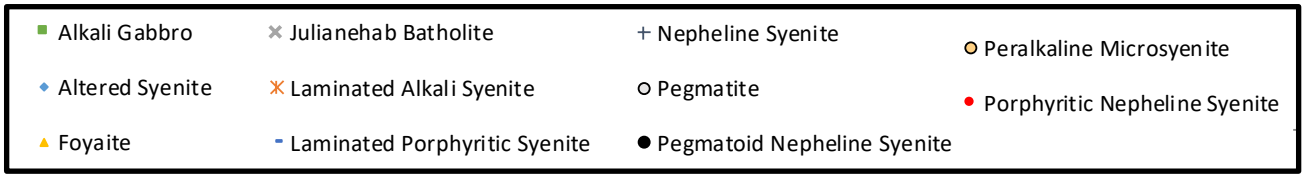

Figure 7 indicates the conditions needed within the MAMC produce mineralized and none mineralized samples in terms of peralklalinity, silica saturation, formation and rock type. In general, NTZR mineralized samples are restricted to MSF (+GF) peralkaline microsyenites (+ some pegmatites, syenites and altered syenites). Mineralized silica saturated and undersaturated samples are seen and this is discussed later with regard to regional distribution.

5.3 Trace element spatial distribution

The NTZR have been plotted spatially in figure 8Figure , on a greyscale map of the MAMC (for a color high resolution map see Figure 2). Spatial relations of element concentrations are consistent across each element. Figure 8 C - F show the higher concentrations are found in three main areas towards the edges of the MSF, when in/ or near a contact with the basement rock or the GF, they are also intimately associated with sheets of peralkaline microsyenites (See Figure 7 and figure 2). These sheets are found in the GF (North east) and in the MSF in the south west. Elevated values are also found in both the peralkaline sheets and microsyenites to the south west below the Sermeq Qiterleg river. This has been denoted as three areas of NTZR mineralization outlined in Figure 8 A. These areas of high concentrations indicated in Figure 8 C-F however do also contain samples that have low concentrations of these elements. Conversely, low concentrations of these elements are found towards the center in nepheline syenites of the FDF and MSF, away from the outer contact. There seems to be no relation to increased concentrations with the ring dyke intrusions or correlation with faulting.

It is clear from the field observations that the development of the mineralized samples is linked to the development of the samples named ‘peralkaline microsyenites’ (Figure 7). It must also be noted that these regions are generally towards the edges of the MSF, and GF when in contact with the basement rock or within the altered syenite halo at the edge of the MAMC. The peralkalinity of these locations has also been plotted Figure 8 B showing that strongly peralkaline rocks do overlap with areas of NTZR especially towards the edges (N/SE and SW especially). However, there are areas, towards the south and center where there are also peralkaline samples with no mineralization.

Modal qtz (wt.%) and modal ne (wt.%) is also plotted spatially to see how it relates to the NTZR mineralization. It appears that samples with both quartz normative or nepheline normative minerology are present in the mineralized samples. Similar to the peralkalinity concentrations do have some, not significant, relationship to silica content. The

FDF, within the center, is silica poor causing a core of normative nepheline running from NW-S. The three zones of mineralized samples in figure 8-C have differing normative minerology. To the west there is a more nepheline normative minerology while the east there is more quartz normative. Moving towards the edge of the intrusion the silica content increases. There seems to be an east-west divide, with more silica rich to the east, and more silica poor to the west as seen with more quartz normative to the east and nepheline normative to the west. The most silica rich samples lie at the edge of the MAMC towards the contact with the basement rocks and GF.

The peralkaline microsyenites and sheets that have elevated concentrations of trace elements are located only in the MSF and GF and strike parallel to the outer contact. The central FDF is undersaturated in silica, a low peralkalinity index and low trace element concentrations. The peralkaline sheets which seem to have an intimate connection to the trace element concentrations do not cut into this unit and are restricted to the MSF and GF indicating they are formed from the intrusion of the MSF.

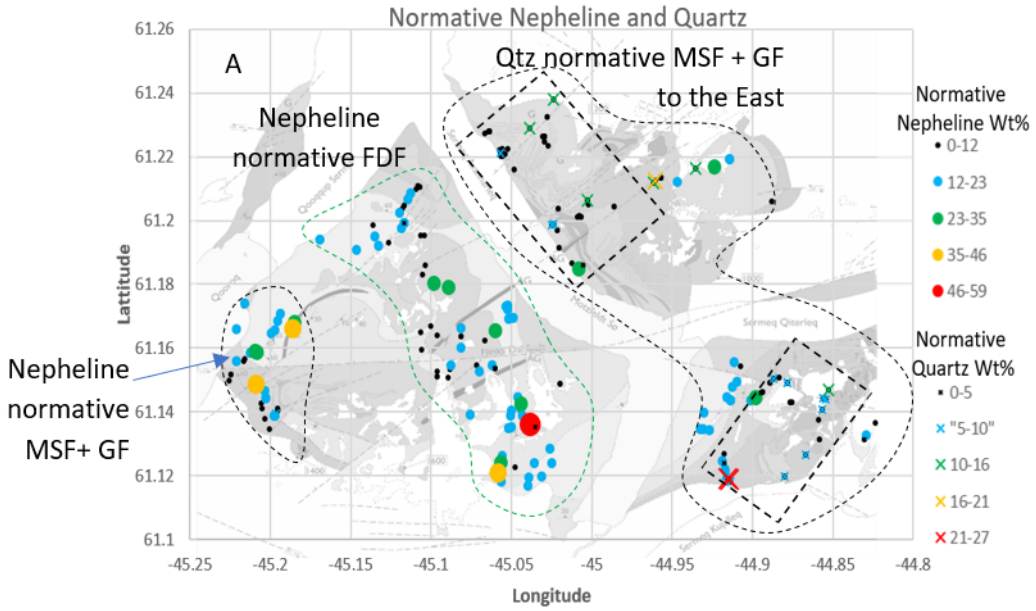

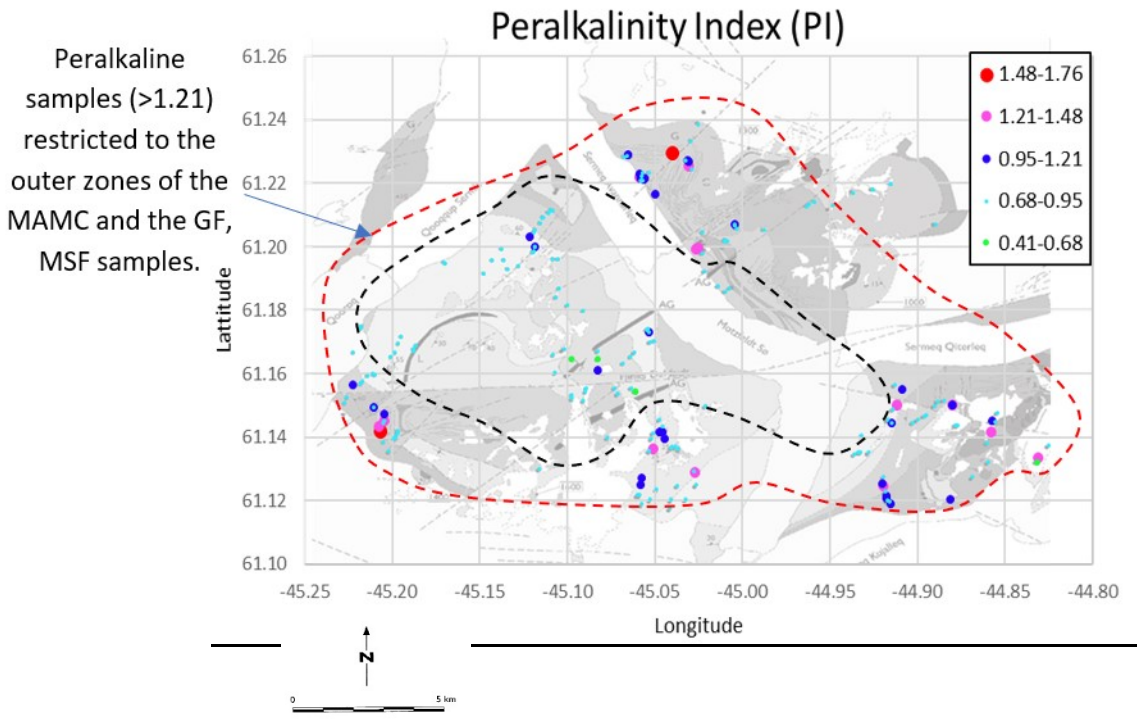

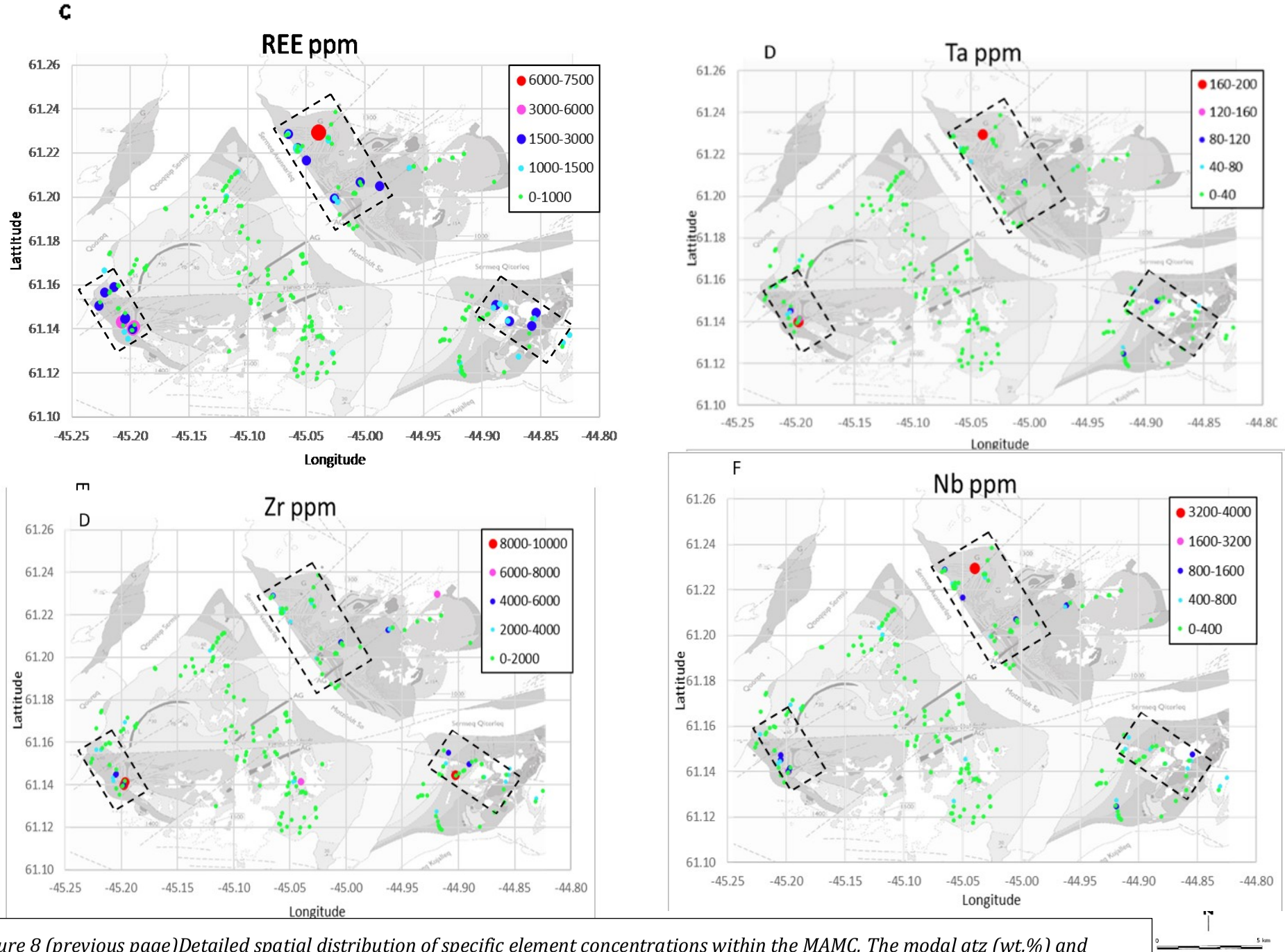

Figure 8 (previous page)Detailed spatial distribution of specific element concentrations within the MAMC. The modal qtz (wt.%) and modal ne (wt.%) nepheline and quartz has been plotted in figure A. In figure B the peralkalinity index. Nb, Zr, Ta and REE are in ppm Figure C-F. REE represents the elements La ppm, Ce ppm, Nd ppm, Sc ppm and Y ppm as these are the only elements samples in this dataset.

6. Discussion – Regional data set

6.1 Geochemical evolution of the MAMC

The geochemical evolution of the MAMC can be tracked through the changes in chemical composition between the three formations. Blaxland et al. (1978), Upton and Emeleus (1987) and more recently, Upton et al. (2003) and McCreath (2012) have shown through radiometric dating and stratigraphic relationships that the GF is the oldest unit, the MSF the middle, and the FDF the youngest (figure 3). Following this age progression, the data show distinct trends in chemical composition for the intrusive units of the MAMC.

Rock classification shown on the QAPF diagram (figure 4) show that the rock units evolved from a more quartz dominated GF (ranging from quartz-monzonite to foid-bearing monzonite) through a variable MSF (ranging from silica saturated monzo-granite to foid-monzosyenite) to a silica undersaturated FDF (ranging from foid-bearing monzonite to foidolite). Although this change in chemical composition between the formations is not evident in the hand sample descriptions they clearly show a variation in chemical signature. This classification also shows the variability and similarities between the formations. The GF, and FDF are classified as quartz rich and quartz poor respectively in figure 4, show relatively little overall chemical variation within their respective zones. Narrow band of samples are grouped in two main areas (monzonite zone (green in figure 4) and foid-monzosyenite zone (red in figure 4)). The MSF on the other hand shows a much larger variation with samples that have normative minerology that are both quartz rich *and* poor, and also include samples that are rich in alkali feldspar or rich in plagioclase. This is illustrated by the expansive blue zone in figure 4.

This chemical evolution and variation is also mirrored in the TAS diagram of figure 5 with the SiO_2 content of the samples decreasing with age, whereas the total alkali content (Na_2O+K_2O) increases. Figure 5 follows an evolution pattern from syenite in the GF and MSF to a foid-syenite in the FDF. Broadly the data also group into two main zones 1) high SiO_2 with low Na_2O+K_2O and zone 2) low SiO_2 with high Na_2O+K_2O, denoted by arrows in Figure 5. The evolution of the MAMC traverses from zone 1 (GF) to zone 2 (FDF) with a transitional phase overlapping both zones with the MSF. The geochemical signature of the FDF which shows little variation and comparatively low NTZR values. Potentially, external factors other than magmatic differentiation occurred during the emplacement of the MSF and the GF to cause an increase in silica and decrease in total alkalis compared to that of the FDF

The MSF in particular shows a highly variable geochemical signature, it has examples with geochemical signatures similar to that of both samples of the GF and FDF supporting the interpretation that the MSM may have been a transitional phase between the two formations. Spatially the mineralized samples are restricted to the MSF and GF and are related to the development of the samples labeled as ‘peralkaline microsyenites’.

6.2 Petrogenic controls on Nb-Ta-Zr-REE enrichments in the MAMC

Trace elements were analyzed to find the compositional changes between the three formations. It is apparent that the MSF and GF are much more enriched in NTZR, with the MSF having the most enriched samples. The younger FDF has the lowest enrichment of trace elements.

This NTZR mineralization is plotted against peralkalinity Figure 7 and shows a poor correlation between the formation it is derived from. This is also plotted in Figure 6, the similarity of the alkalinity of the three formations indicates that there was very little change in the degree of magmatic differentiation during the three periods of emplacement. The source of the MAMC therefore evolved similarly during the emplacement of all three formations and that the source compositions and evolutions were relatively similar. Although some samples of the MSF and GF have been somewhat enriched in trace elements the variable peralkalinity index does not fully support a scenario where this enrichment is derived solely from an evolving source.

Spatially, the mineralized zones do overlap with peralkaline fringe of the MAMC noted in Figure 8-C except in one region the south Figure 8-B. The mineralized samples lay in peralkaline sheets in regions of geochemically alkaline rocks but importantly in MSF samples. The peralkaline samples in the south that have no mineralization are found in the FDF and have not undergone the same enrichment that is found in the mineralized samples of the MSF. The mineralized samples seem to develop in areas where there are also peralkaline rocks being formed, normally towards the contact zones and are associated with the development of peralkaline microsyenites sheets of the MSF. However, a consistent overlapping peralkalinity signature of the three formations, as seen in figure 6 suggest that further controlling factor in concentrating these elements into these zones rather than fractionation. The contact with the outer contact in three main zones (Figure 8-C-F) and the development of peralkaline microsyenites of the MSF seem a likely source.

The consistent geochemical signature of the FDF could represent the true composition of the MAMC while the GF and the MSF that have highly variable geochemistry are examples of samples that have partially undergone some syn to post-emplacement compositional modification. This is in line with the noted field observational data of highly altered samples towards the contact edges. Spatially the west and center of the MAMC (figure 8-A) is more nepheline normative signature which covers the western MSF and FDF. While in the east a quartz normative signature is dominant in the GF, and eastern MSF. This silica enrichment has caused a quartz normative signature that can be considered anomalous from the ”fresher” signature of the FDF. This could be linked to the samples association with the outer contact, since assimilation and interaction of the intrusion with the country rock could give rise to a more silica rich geochemical signature. This may be the cause for the composition pattern within the MAMC with a normative quartz altered halo at the eastern edges and a normative nepheline core (outcropping in the FDF at the center and the unaltered MSF to the west) where interactions with country rock was limited (Figure 8-A).

Figure 7-A-H and figure 8-A shows that the mineralization is independent on SiO_2 saturation level but is spatially related to variations in SiO_2. However, a certain threshold of peralkalinity appears to be required Figure 7-Q-X since mineralization is restricted to samples with a PI >0.9 and mineralization is also seen is co-incidental. The

Rb/Sr ratios have also been plotted in Figure 7 I-P as an indicator of intensive late- to post-magmatic alteration leading to a redistribution of Rb and Sr as seen in the llimaussaq intrusion (Sørensen, 1997) but this ratio does not correlate with mineralized samples and indicates that intensive late- to post-magmatic alteration was not involved in NTZR concentration.

The key to understanding the mineralization may lie with its association with the rocks noted as 'peralkaline microsyenites' and that these seem to have a relationship with the outer edges of the MAMC. The mineralization was apparently not concentrated through differentiation and fractionation of feldspars as seen in llimaussaq. There was some other process at work.

It is seems likely that there has been some interaction with the country rock and assimilation of SiO_2 and although not normally mobile in the fluid phase, recent studies have shown that under the right conditions NTZR elements can become mobile in very late stage orthomagmatic fluids (Rolland, et al., 2003). It has been shown that these fluids can be important in the transport of REE, since they contain complexing volatile agents such as F, Cl. Also, CO_2, SO_2, H_2S, HCl, and possibly HF can cause the REE to devolatilize liberating them from the melt phase into the fluid phase (Rolland, et al., 2003). The interaction between the country rock and the fractionating magma may supply the elements needed to mobilize the NTZR elements into late stage fluid phases. This combined with the intrusion of the late stage peralkaline microsyenites derived from the fractionating magma, may be responsible for th formation of mineralized zones. However, this concept may be beyond the scope of this study and needs to be investigated further.

6.3 Regional summary

A regional summary of the MAMC intrusion is provided in figure 9. From the geochemical data it appears that the GF and FDF intruded to a depth in the crust where it began to interact with silica rich rocks of the Eriksfjord formation (figure 9 A and B). This interaction with the country rock increased the silica content of the rocks and incorporated other elements such as F, Cl and other volatiles. Late stage magmatism of peralkaline microsyenites of the GF and mainly the MSF, already enriched in trace elements from an evolved peralkaline source, were further enriched by orthomagmatic fluids that were circulating around the country rock and intrusion, the incorporation of volatiles from contamination by the basement rocks caused the trace elements to become mobile and enrich into fluids associated with the sheet intrusion of late stage peralkaline microsyenites (B). The product was the development of an enriched outer domain with microsyenites, pegmatites and altered syenites held mainly within the outer edge of the MSF (B and C) while the inner edge was unaltered and unmineralized.

Finally, the FDF intruded into the center of the MSF (C) by intruding to a shallower depth in the crust and being shielded by the much larger MSF. It did not experience the contamination and assimilation of the country rock and the enriching orthomagmatic fluids and the addition of silica did not occur hence preserving the composition of its original source.

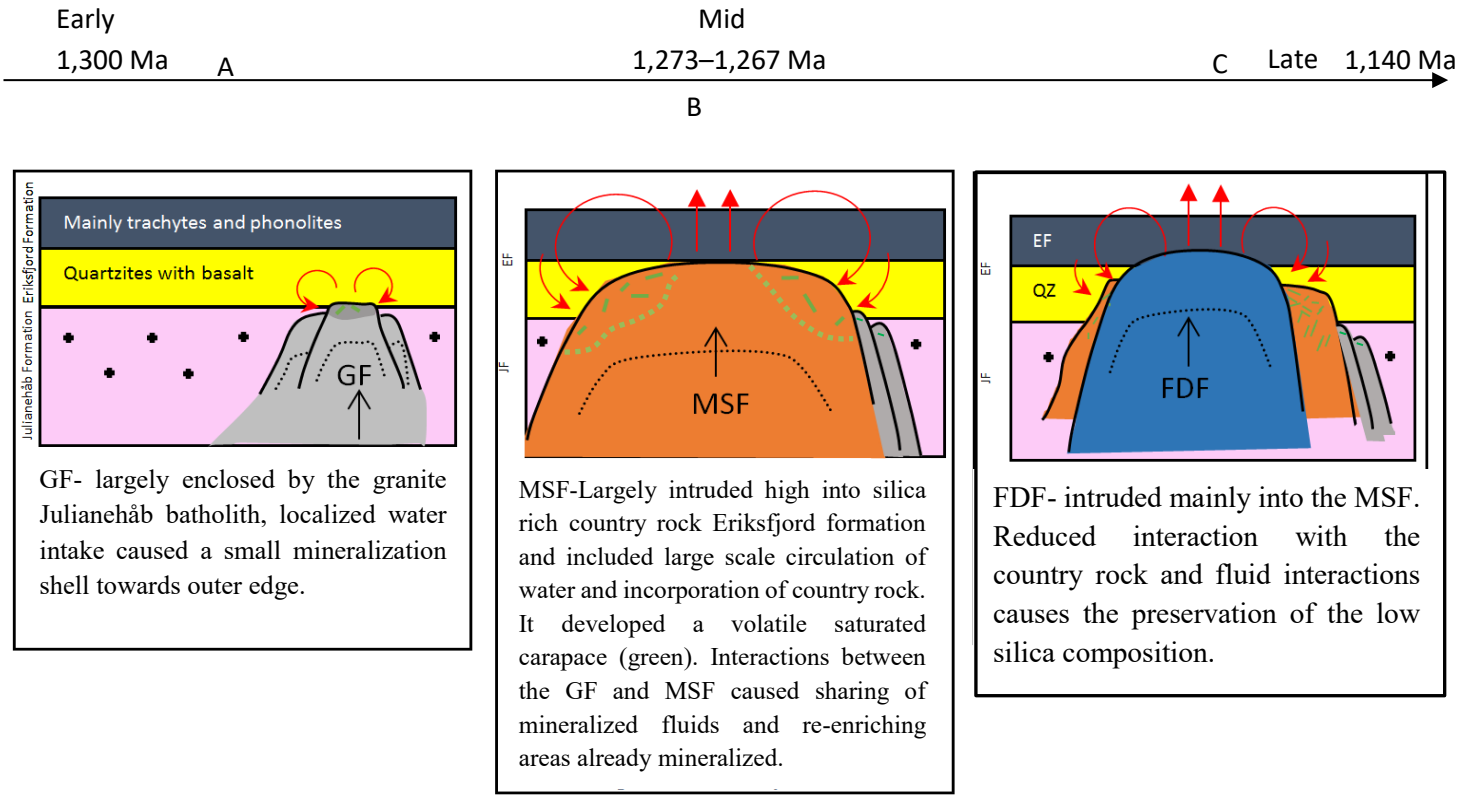

Figure 9 Development of the MAMC and interaction between the different intrusions. Developed and based on (Bradshaw, 1988) using own data and information to infer development of mineralization. Pink: Julianehåb batholith, blue-grey/yellow: Eriksfjord formation, grey: GF, orange: MSF, blue: FDF and green: development of microsyenite sheets and NTZR mineralization.

7. Outcrop scale investigation of the Stoorelv valley.

7.1 Outcrop description and sample locations

The second section of this thesis focuses on an outcrop scale investigation of select samples from the MAMC. Field data of 14 hand samples were collected by Samuel Weatherley of the Geological Survey of Denmark and Greenland(GEUS), in the summer of 2016 (Table 2). The samples are derived from a syenite unit of the GF in the Stoorelv valley (See map in figure 12 for specific locations) in the north east of the MAMC. This is characterized by an association of peralkaline microsyenites and pegmatites. The Stoorelv valley is composed mainly of the coarse-grained syenites. Peralkaline microsyenites associated with late stage magmatic fluids of the MSF run through this valley in sheet like intrusions cutting the syenites (figure 12). The Stoorelv valley exposes repeated peralkaline microsyenite sheets, banded syenites and syenite layers and their contact relations (see outcrop photo and stratigraphic log in figure 13 for further details and stratigraphic relationships). The samples of this outcrop can be split into three rock types: syenites (section 7.2), microsyenites (section 7.3) and pegmatites (section 7.4).

Figure 13 shows an outcrop photo, which is split into 10 units. These are labeled L0-L9 and 14 samples were taken from these units and the contacts between them. The photo identifies the sample locations, the graphic log shows the stratigraphic relationship of these samples. The graphic log also illustrates field data regarding the variation in grain size, and contact relationships between the layers. There is some variation in the layer thickness with the bounding syenites L1 and L9 being larger (6-10m) while the inner microsyenites L3, L5, and L7 are thinner (1-2m). The thick microsyenites L1 is cut by thin veinlets within the layer and is bounded by coarse grained pegmatites. Associated with these thick microsyenites units are fragmented-contacts especially when in contact with the layered pegmatites (see L6 and top of L8 in figure 13). There is also indication that there has been interaction between the microsyenites and the syenite with strings of the syenite within the microsyenites of L3. Layers 4, 6 and 8 show layered pegmatites running through the rock units that are especially related to fragmented contacts.

The microsyenites have a smaller crystal size (1-3mm) while the GF syenites are much coarser (5-20mm). Often, at contact zones of the layers there is a very coarse (>1 cm) pegmatite vein. The contacts of the thickest microsyenite units often show fractured contacts that are often filled with pegmatite. The coarse grained syenites exist as lenticular rafts (10s of meters) aligned long axis parallel and are surrounded by the microsyenites and pegmatites. The unit is also periodically cut by layered syenites or layered pegmatite units (Weatherley, 2016).

Table of rock samples taken from the Stoorelv valley.

Sample Number	Rock Description	Layer (L0-L9)
562123	Syenite	L9
562122	Heterogeneous course grained syenite	L8
562121	Heterogeneous fine grained syenite	L8
562120	Microsyenite	L7
562119	Microsyenite above the pegmatite	L5
562118	Syenite and pegmatite	L4
562117	Contact between the lower syenite and the microsyenite above	L2-L3 contact
562116	Syenite directly above the L1 and L2 contact	L2
562114, 562115	Pegmatite contact	L1-L2 contact
562113	Microsyenite	L1

562111 & 562112	Pegmatite contact	L0-L1 Contact
562110	Corse grained syenite	L0

Table 2 Rock description table of all field samples taken from the Stoorelv valley outcrop including: sample number given by the GEUS, rock name/description, stratigraphic relationships derived from field observations.

7.2 Syenite field descriptions and petrography.

The syenites of the Stoorelv valley are represented by the samples taken from L0 (sample number 562110), L2 (562116), L4 (562118), L8 (562121 and 562122) and L9 (562123). Samples from the: L0, L2 and L9, are examples of massive coarse grained syenite. In hand sample it is pink-buff colored with occasional internal cm scale pegmatites. There are examples of internal pegmatites containing up to 20 cm amphibole and feldspathoids which are arranged parallel to trend of the contacts between microsyenites, syenite sheets and rafts. The syenites from L4 (562118) and L8 (562121 and 562122) represent a much less massive and more layered syenite with greater relationship to pegmatites and they are visually different to the massive L0, L2 and L9. L8 in particular is heterogeneous, has layered internal syenites (Figure 10) and show multiple generations of pegmatites. The sample taken from L4 is a from a syenite-pegmatite contact, the layer 4 contains 10 cm leucocratic pegmatite horizons which increase in abundance towards the top of the layer.

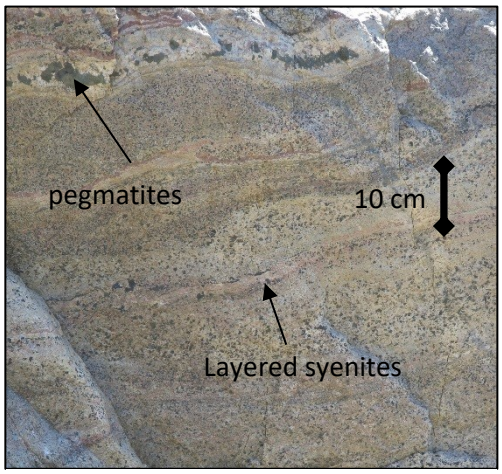

Figure 10 Outcrop photo of heterogeneous syenite and pegmatites, cm scale layering within L8.

Macroscopically, the samples can be described as felsic, coarse grained (5-20 mm) syenites with mafic agglomerates scattered evenly within the matrix. The felsic (nepheline and feldspar) component accounts for ≈ 80% while ≈ 20% is mafic (green - black spots of amphibole and clinopyroxene, figure 11). It is composed predominantly of bladed K-feldspars, orthoclase (~40%) pinkish-white in hand sample and randomly orientated. Under UV light the samples have a deep red fluorescence indicating a presence of sodalite.

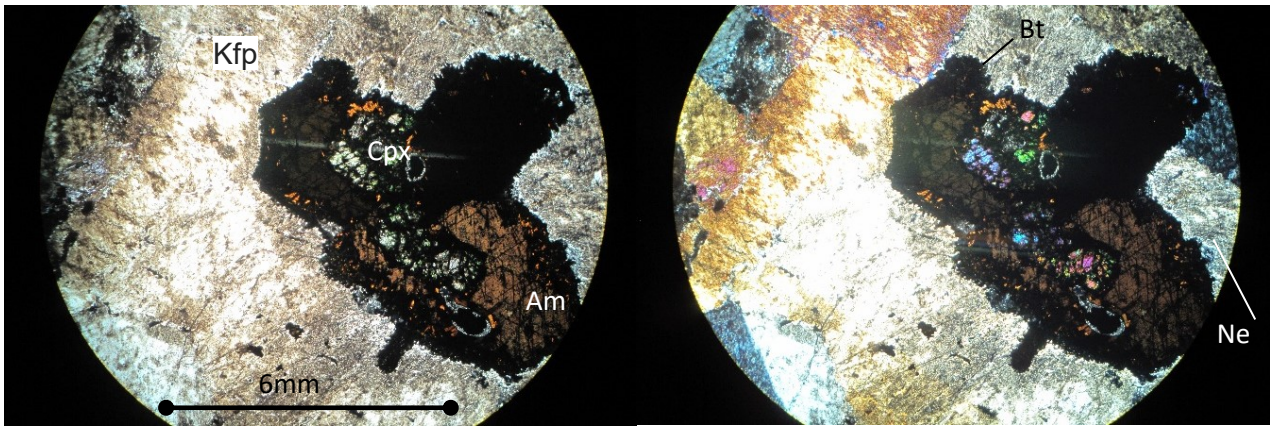

Figure 11 Sample 562110, mafic aggregate of clinopyroxene, amphibole and a rim of biotite and ferro-katophorite with surrounding crystal matrix of plagioclase and nepheline 12 mm diameters. PPL on the left XPL on the right.

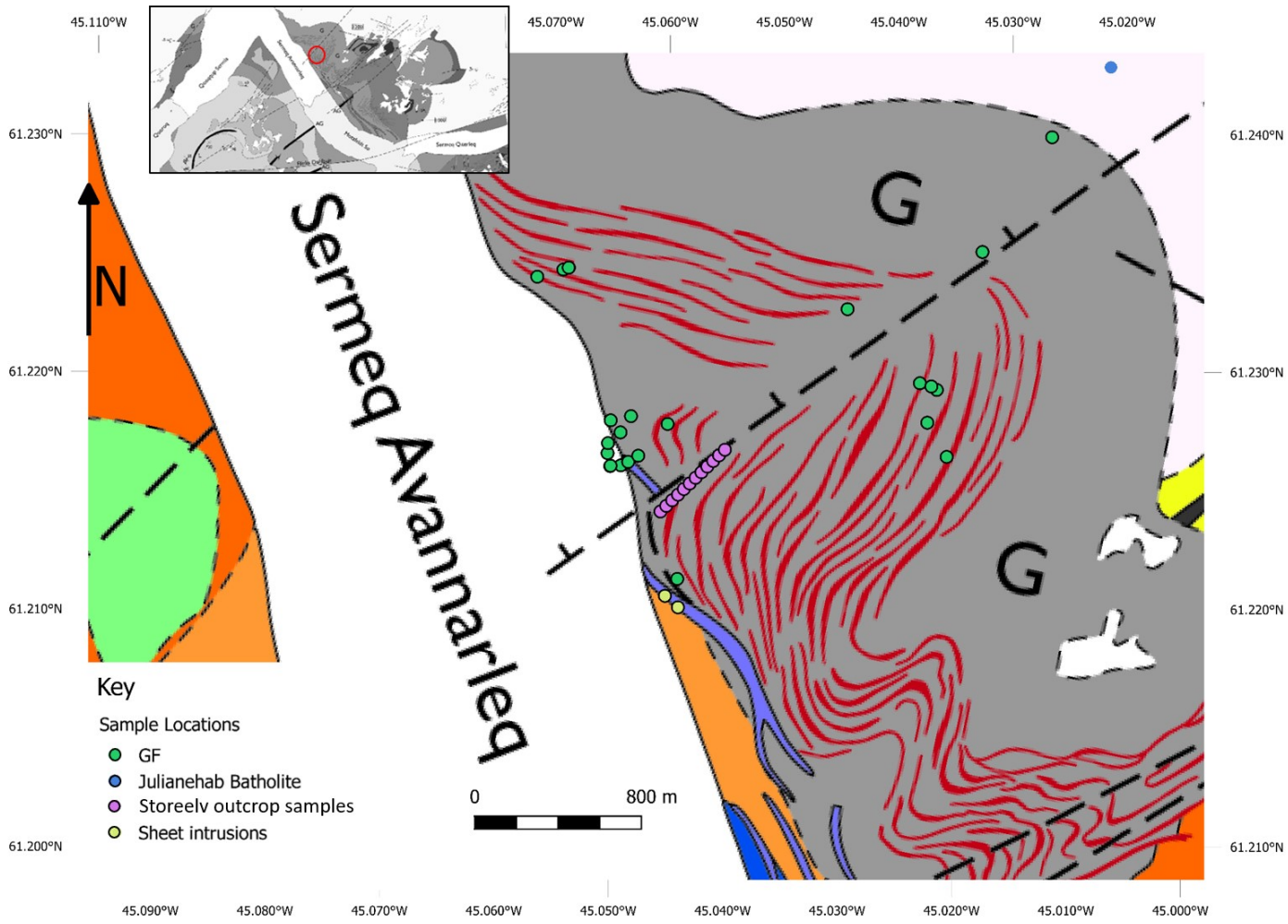

Figure 12 Enlarged geological map of the Storeelv valley showing outcrop sample locations (purple) and other sample locations of LML database 1984 within the Stoorelv Valley.

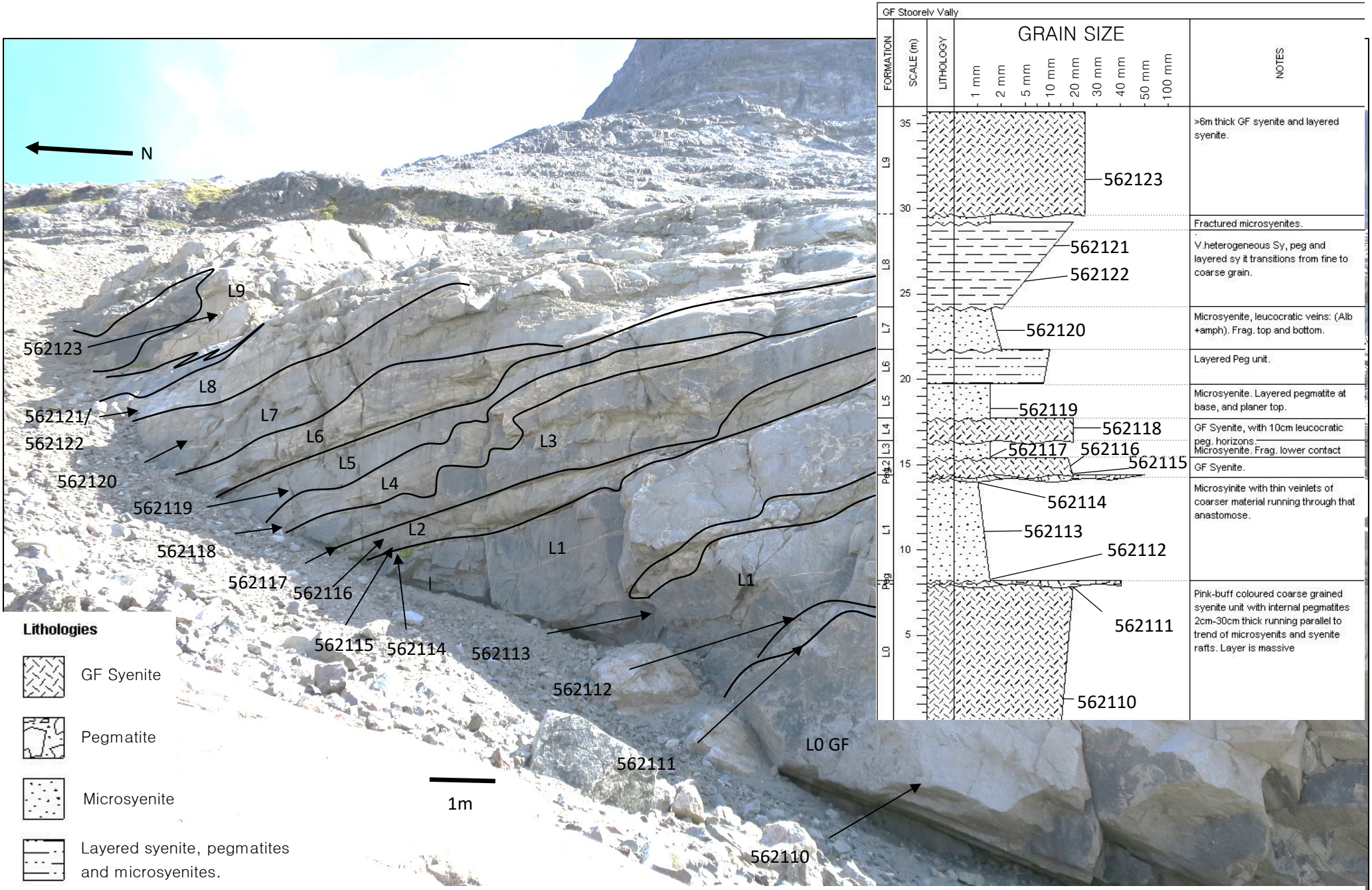

Figure 13 Outcrop photo showing sample locations and defined layering seen within the unit. Top right shows a graphic log of the outcrop with estimated sample locations within each layer, grain size, and notes on each layer.

In thin section, the feldspars account for 40% of the crystal mass. They have very poor simple twinning with first order; grey-dull orange birefringence. Nepheline accounts for roughly 30% of the rock matrix and shows low relief, mottling, and low 1st order grey birefringence. The other important component are the mafic agglomerates that are evenly distributed within the matrix consisting mainly of subhedral- anhedral amphibole (brown-dark brown with pleochroism often showing an alteration rims) that is accompanied by clinopyroxene and minor biotite.

Often the nepheline and orthoclase have complex intergrowth at the grain boundaries and alteration textures such as thin growths of high birefringence sericite following cracks, contacts and twinning lines in the grains. Rare hexagonal high relief prisms of trace apatite are also noted.

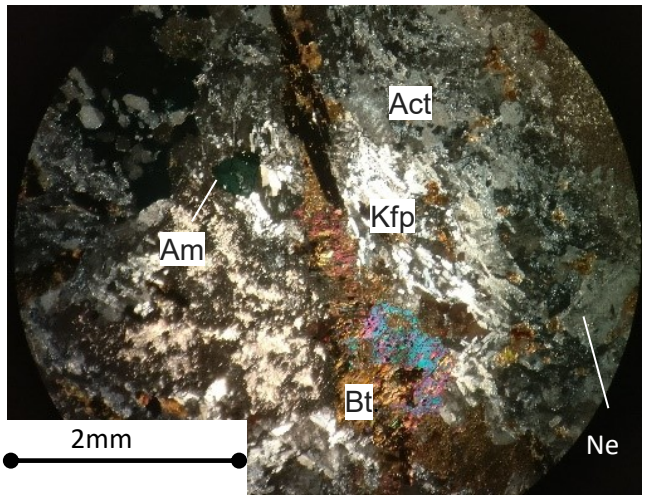

Figure 14 562122 XPL. 5.5mm Large amphibole crystal completely replaced with fine grain biotite. The matrix of feldspar and nepheline altered and contains actinolite

Samples closer to pegmatites and contacts such as 562116, 562118 and 562122 (Figure 14) are noticeably more altered and have markedly less clinopyroxene. The mafic agglomerates have developed cores of biotite replacing clinopyroxene and amphibole. The feldspars also seem to be more altered with twinning hard to distinguish and the grain boundaries indistinct and showing a mottled fine-grained alteration of actinolite. Sample 562122 especially is altered showing many particular textures such as thin elongated and large (1cm) crystals of amphiboles and re-crystallization of actinolite in the feldspars. Some nepheline show a radiating habit and subtle birefringence. Some of the lager amphiboles has been pseudomorphed by fine grain biotite. Absent from these syenite units are any notable concentrations of minerals that carry the mineralization such as pyrochlore zircon or bastnäsite.

7.3 Microsyenite petrography and field descriptions.

The microsyenites of the Stoorelv valley are represented by the samples taken from L1 (sample number 562113), the contact between L2 and L3 (562117), L5 (562119) and L7 (562120). The microsyenites are closely associated with pegmatites or brittle fragmentation at the contacts between the layers. The layers range from cm to m scale. The thicker layers are typically associated with fragmentation along contacts and can even be disintegrated, occurring as blobs within pegmatites (Weatherley, 2016). The rock is mainly comprised of feldspar and nepheline (~65%, figure 15), much of this has been altered with actinolite destroying much of the crystal structure. Broken anhedral biotite and amphiboles make up the main mafic minerals. Some elongated 3-4 mm amphibole crystals (figure 17) cut through the fine grained

groundmass and show similar orientation within many samples. The alkali feldspar is bladed and forms most of the groundmass and also often shows a distinct orientation lining up the long axis.

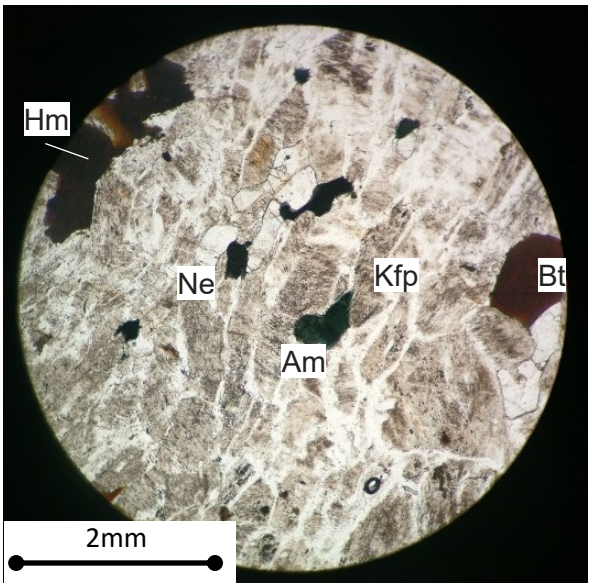

Figure 15 Microsyenite 562119 in PPL composition fine grain feldspar and nepheline makes up the main groundmass the mottled pattern of actinolite alteration. Fine grain nepheline and anhedral arfvedsonite lie in the center and biotite to the right of the image, dark brown semi-isotropic mineral hematite to the top

The microsyenite layers have several interesting features (figure 13, graphic log) L1 contains xenoliths derived from the surrounding GF Syenite. While the L3 contact is fragmented with the microsyenite contact contains pegmatite, the layer in general has the appearance of 50cm fragmented blobs rather than a continuous sheet. L7 shows leucocratic 2-2.5 cm thick albite and amphibole veins within the middle of the layer (figure 16).

Arfvedsonite is common in microsyenites as fresh fine (1-2mm) euhedral crystals. These are found in small clusters with biotite and accompanied by other species of amphiboles spread evenly throughout the groundmass and some trace semi-isotropic euhedral hematite (figure 15). There are some, rounded and highly altered fine grain feldspar pseudomorphs of olivine xenocrysts present.

Samples taken close contacts are distinctly more altered sample 562117 is the prime example of this. Here, the microsyenites have elevated concentrations of NTZR bearing minerals such as pyrochlore and trace zircon which are present in clusters (Figure 17b). In addition hematite is a common mineral. Sample 562117 lies directly at the highly fragmented boundary between L2 and L3 (figure 17). Amphiboles (upto 5-10 mm in length) have been altered to a fine grain matrix of biotite. There are some pseudomorphs of clinopyroxene but these mainly have been altered to a fine grain biotite. Associated with these altered amphiboles are an abundance of very fine grain (0.01mm) isotropic minerals that could be REE bearing pyrochlore. The altered microsyenites have feldspar grains which appear to have begun to re-crystalize from the amphibole "eating" into the larger amphibole grain boundaries (figure 17 image A).

Figure 16 albite and amphibole veins within the middle of the layer 7.

These elongated large amphiboles are not seen in every microsyenite sample, and the different samples show variations in the amount and type of alteration. The samples 562119 and 562120 for example are taken from the center of the units and shows a lot of alteration by actinolite and fine grain amphibole (figure 18). Here, biotite growth and fine grain isotropic pyrochlore(?) that is seen in samples close to the contact zones, are absent.

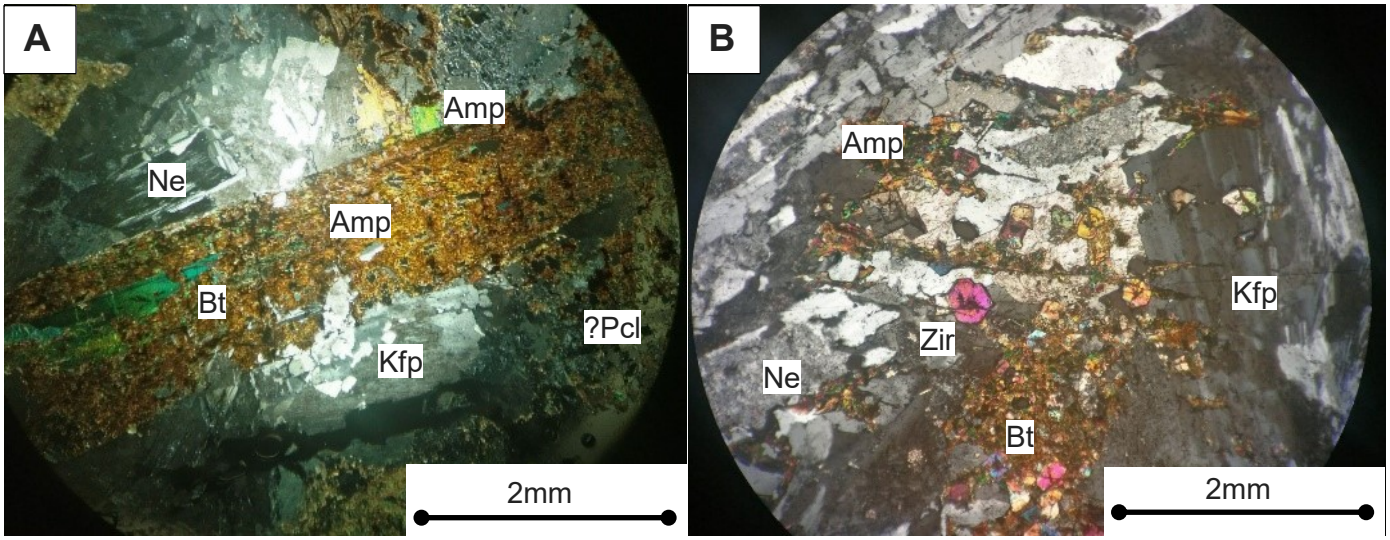

Figure 17 A) Sample 562117, XPL showing almost full alteration and destruction of large amphibole (Am)crystal to a fine grain biotite (Bt) matrix. Note little alteration to the nepheline (Ne) feldspar (Kfp) matrix and the very fine grained isotropic areas in the right side composed of pyrochlore (Pcl). This texture is common in altered samples. Also, note the growth of feldspar 'eating' into the large amphibole grain. B) Sample 562117, XPL showing a cluster of well-formed zircon (Zir) crystals which have grown in an alteration texture of amphibole and biotite along fractures between K-feldspar and nepheline.

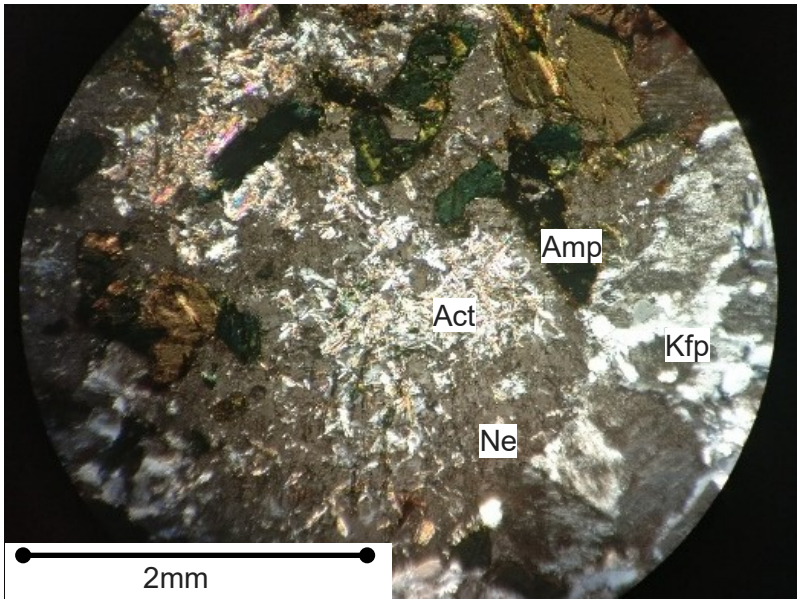

Figure 18 Sample 562120 right XPL, fine grain matrix of alkali feldspar(Kfp), nepheline (Ne) and amphiboles (Amp) with some alteration to biotite. The main section is dominated by an altered nepheline crystal that is now dull grey and filled with fibrous actinolite showing a radiating habit and subtle birefringence. It is pale green in PPL and represents replacement at the center of altered grains.

7.4 pegmatite petrography and field descriptions.

The pegmatites from this outcrop are represented by samples taken from two large pegmatites that occur between the syenite L0 and the microsyenite L1 (sample number 562111 and 562112), and the upper contact between L1 microsyenite and syenite L2 (562114 and 562115). The lower pegmatite (figure 19), between L0 and L1 is 20 cm thick, and coarse grained (5cm). Major constituents are albite, calcite, alkali feldspar and amphibole. There are also miarolitic cavities. At the upper contact between L1-L2 there exists another 20cm pegmatite between the lower microsyenite and the syenite above. It is very similar to other pegmatites, showing very coarse grained 3-6 cm calcite and amphibole and alkali feldspar.

Both set of samples have a distinctive pegmatitic textures consisting of large interlocking crystals, with some greater than 2.5 cm. The thin sections display a pegmatitic texture, of oriented fine grained albite (~0.45 mm) with often larger amphibole grains surrounding this. Hand samples glow deep red when exposed to UV light indicating the sample is rich in sodalite.

Figure 19 image of lower 20 cm wide pegmatite between L0-L1 showing large grains of albite, calcite, alkali feldspar and amphibole. The above layer L1 is the fine grain microsyenite and the lower layer is the GF syenite.

Many of the feldspar grains have developed a perthitic texture from subsolidus exsolution of sodic and potassic feldspar (see figure 20). Large (3-5 cm) amphibole grains dominate the structure and at the edges of these grains a fine grained (0.1-1 mm) aggregate of clinopyroxene, amphibole, trace biotite and other indistinguishable mafic minerals have developed (see figure 20). The REE element concentration in these samples are higher than in the other samples from this outcrop. Apparently, the high REE element concentration is held within these isotropic (0.5mm) reddish brown subhedral mafic minerals which are potentially pyrochlore(?) (figure 20 and figure 21) and other fine minerals including zircon, thorite, eudialyte and bastnäsite. In some samples there is re-crystallization at grain boundaries. This re-crystallization is best seen within the pegmatites and some microsyenites close to the layer contacts. The recrystalisation of quartz at the grain boundaries could indicate that fluids were flowing through a crystal mush (figure 22). These aggregates of NTZR bearing minerals particular to the pegmatic samples are responsible for the trace element enrichment compared to the microsyenites and syenites.

The grain boundaries of the larger crystals appear to be recrystallized, while the contacts between the fine grained minerals are sharp. Biotite alteration is persistent throughout the samples especially within larger amphibole grains. The finest crystals are near the boundary contact zones where pegmatite is in contact with the syenite. The dark color and fibrous nature observed in hand sample indicate that the amphiboles are arfvedsonite. All of these contain fine mottling of biotite and fine pyrochlore. Variations in the color of amphiboles indicate changes in Na where there is a

deep blue/green color it indicates an increase in Na. The strong pleochroism seen in the biotite crystals could be due to an increased iron content.

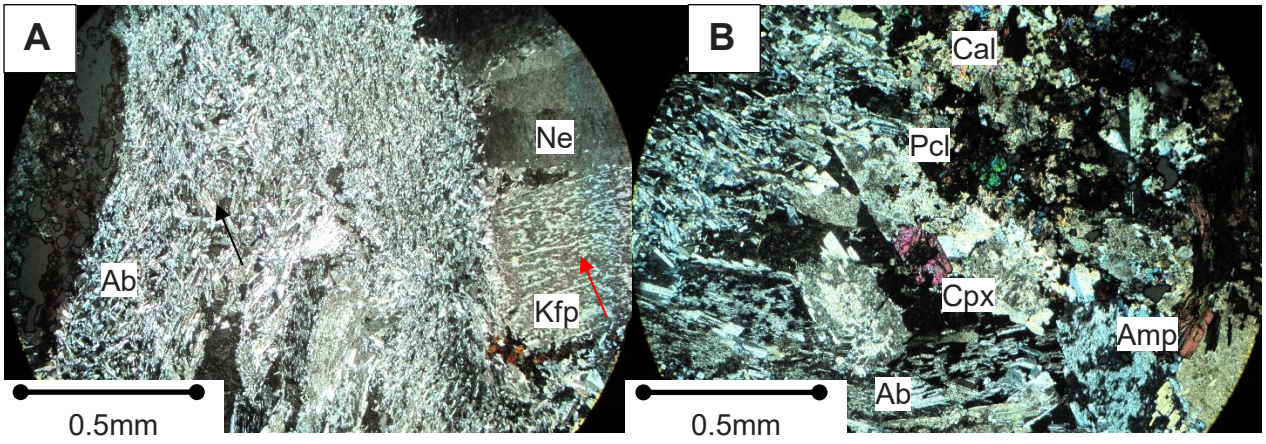

Figure 20 Thin section images of 56111, left XPL showing perthitic texture in feldspars (right red arrow) and the pegmatitic texture of orientated fine grain feldspars running through the center (black arrow). Right image XPL of the aggregate of mafic minerals pyrochlore and other fine minerals including, zircon, thorite, eudialyte and bastnäsite. Clinopyroxene and small amphiboles are next to a large 5cm amphibole grain to the right of the image. Isotropic pyrochlore to the (middle) could account for the increased REE content.

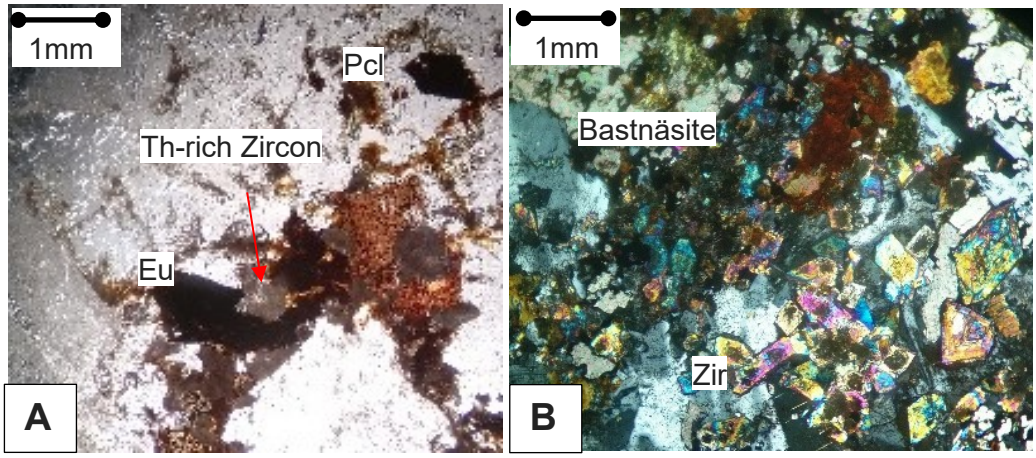

Figure 21 left 562112 Semi-isotropic minerals PPL euhedral pyrochlore crystals, forming aggregate with, eudialyte and Th-rich Zircons. Upper right a euhedral crystal of pyrochlore. Right: 562112 PPL, a cluster of zircon crystals and brownish green intergrows of bastnäsite-(Ce).

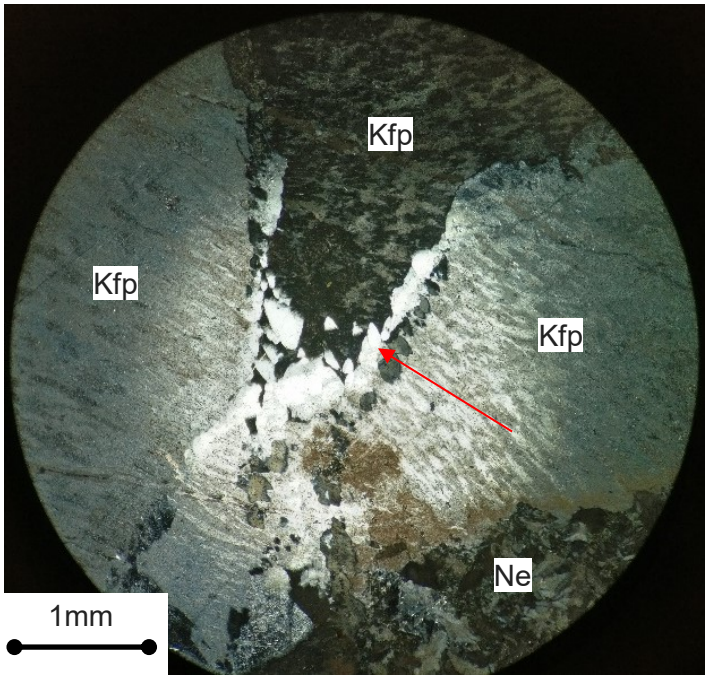

Figure 22 sample 562112: Dissolution at the feldspar grain boundaries causing the re-crystallization of quartz (red arrow) at grain boundaries indicating that there was fluid flow in the crystal mush.

7.5 Outcrop scale major and trace geochemistry.

The three rock types of the outcrop (microsyenites, pegmatites, and syenites) can be effectively distinguished by their geochemistry. The TAS diagram (figure 23) shows the outcrop samples plotted against the samples from the regional dataset for the GF and the MSF. All samples lie conformably within range of the two formations at the syenite, nepheline syenite boundary.

The syenites and microsyenites overly the zone where the greatest concentration of regional samples of GF and MSF is (an average silica of 57% and 58% respectively and an average for of 12% Na_2O+K_2O). While the pegmatites vary in composition, they have similar averages but a greater range in silica and Na_2O+K_2O. 562115 in particular has significantly lower silica and alkali content than the other samples taken from this outcrop. All samples are alkaline and intermediate in composition and are very similar to the regional sample dataset.

The QAPF diagram shows the same regional and outcrop data. They plot in what would be expected of MSF and GF samples, interestingly the pegmatite samples show a range that appears more similar to that of the MSF than the GF. Three syenite samples (562128, 562121 and 562122) are trending towards the foid monzodiorite- being more plagioclase rich and the most undersaturated in SiO_2. All the outcrop samples lie on the boundary of foid syenite- and syenite, with one outlier (562115) lying in the foid monzo-syenite. All of the outcrop samples are SiO_2 undersaturated however the pegmatites and microsyenites are plotting along the SiO_2 saturation line.

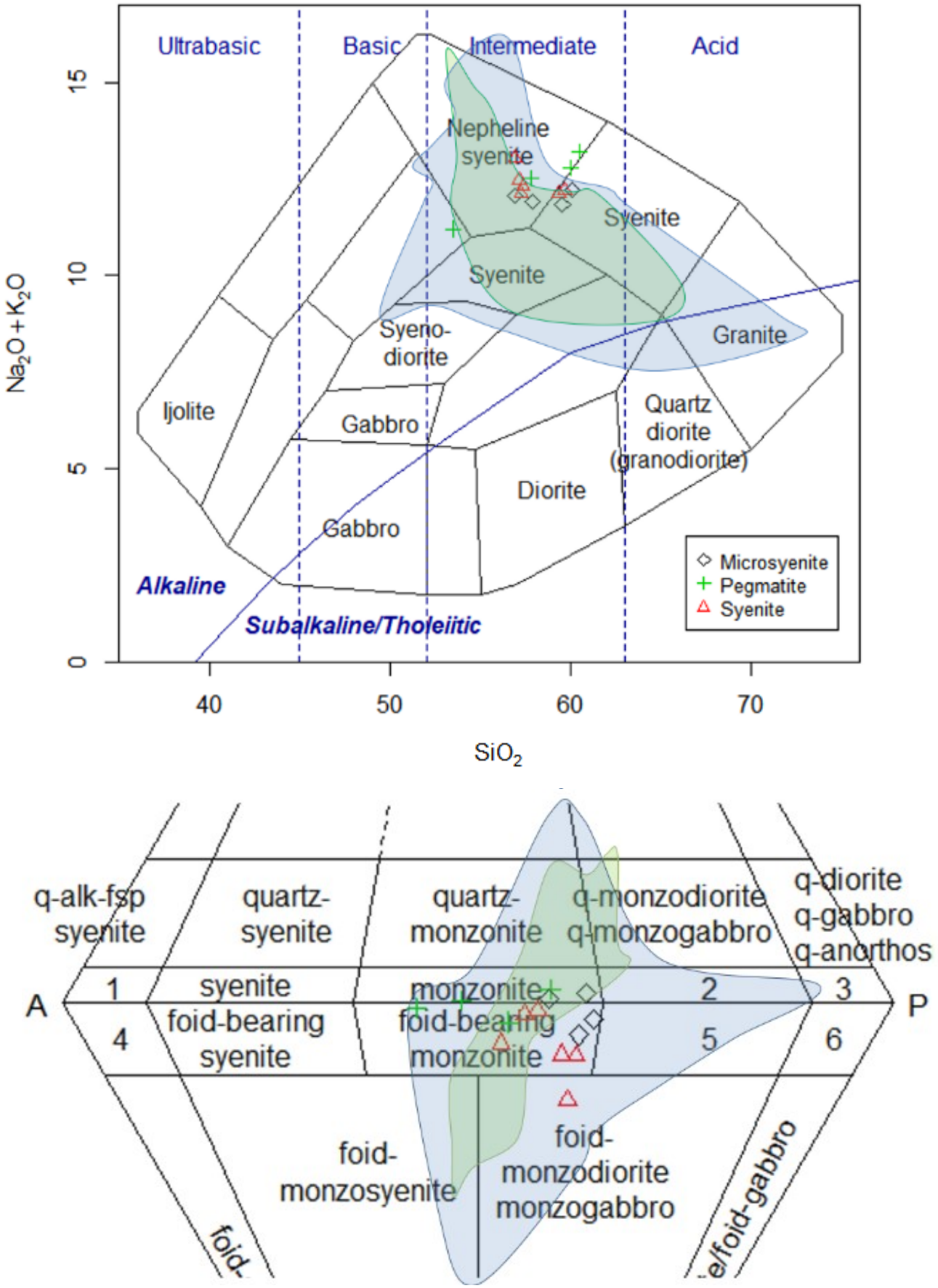

Figure 23 (above)TAS diagram of all outcrop samples divided by the rock type, plotted over the outlines of the regional samples of the MSF (blue zone) and GF (green zone). (Image below) QAPF diagram for outcrop samples

divided by the rock type, plotted over the outlines of the regional samples of the MSF (blue zone) and GF (green zone).

The REE composition of the outcrop samples is shown in Figure 24. It shows a characteristic distinction between the samples that are enriched and those that are depleted in REE. There are clearly two groups of samples, REE poor and REE rich. The samples that are REE rich include the pegmatite samples and one microsyenites (sample 562117) which is taken directly from a fragmented contact between the syenite L2 and the thin microsyenite L3 above.

The REE poor samples include the syenites and the remaining microsyenites. The 'upper' REE-poor samples occupy the middle of the diagram (Samples 562113, 562122, 562121, and 562119 REE 'rich' to poor respectively) are microsyenites, and syenites that are from L8 which is associated with layered pegmatites running through the unit. The lower REE-poor samples consist of the other "fresh" syenites and the syenite 562120 taken from a large microsyenite unit with similar finer grained composition than the syenite.

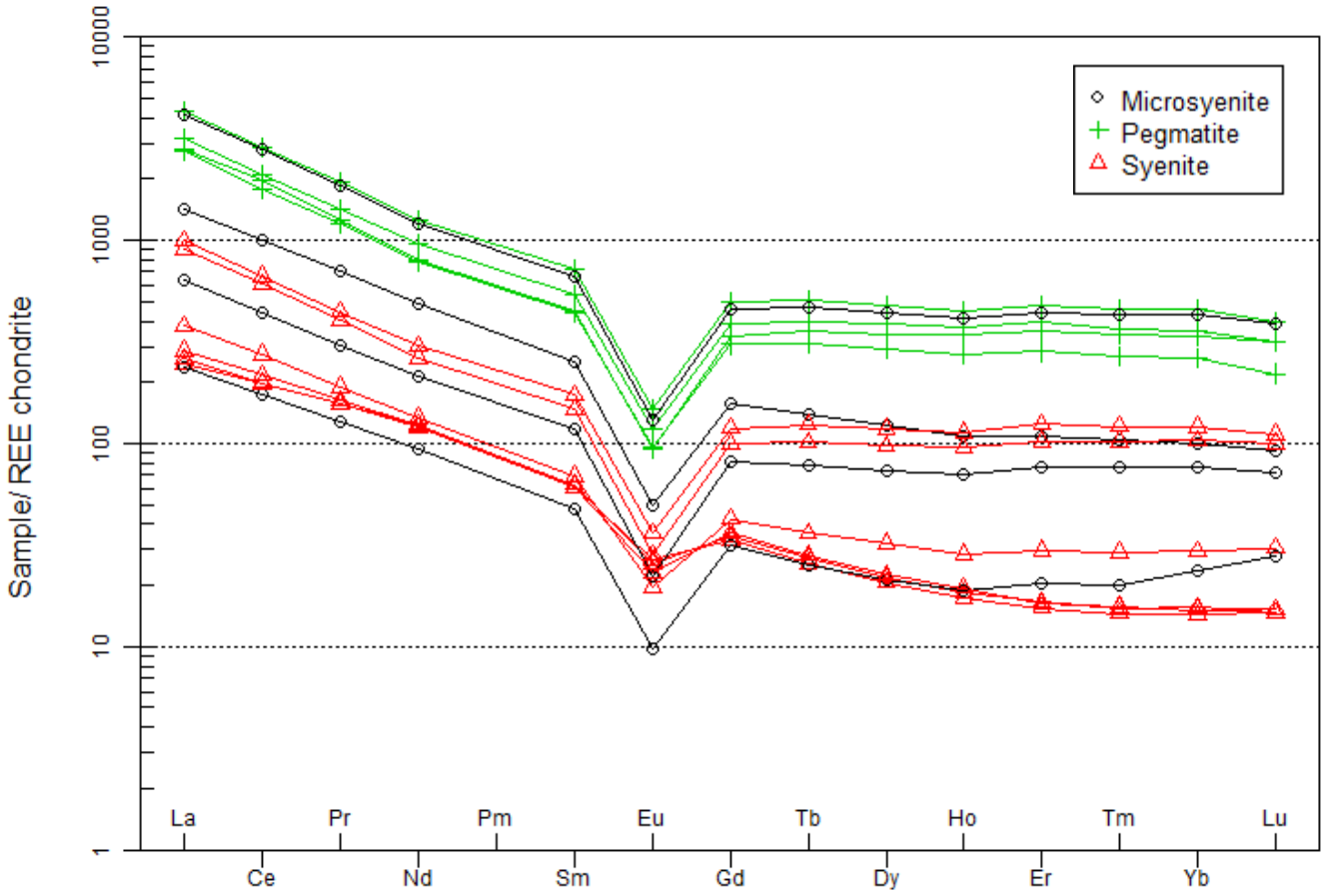

Figure 24 REE C1 chondrite normalized spider plot of all samples taken from the outcrop split by the rock type. The syenites (red) have relatively low REE concentrations while 562121-562122 are slightly more enriched but are the upper heterogeneous layered syenites associated with, layered pegmatites. The pegmatites (Green) are all enriched compared to the other samples as well as the microsyenite 562117 which is taken from the layer contact that is highly fractured. The other microsyenites have average concentrations between that of the syenites and pegmatites except 562120 the uppermost (stratigraphically) microsyenite is anomalous as it has the only enrichment in HREE compared to LREE. The Eu anomaly of all the samples is consistent, apart from that of the sample 562110 and 562123 which are thought to be representative of the syenite of the GF.

The syenite samples 562110 and 562123 can be assumed to be representative of the host Geologfjeld Syenite with low concentrations of REE. Additionally, they have a much lower Eu anomaly compared to the other samples which have more strongly developed negative Eu anomalies. The Eu/Eu* is a measure of this and is calculated by interpolating along the slope from adjoining values for Sm and Gd on a chondrite normalized REE spider pattern. If Eu/Eu* < 1 then there is a negative anomaly as seen in figure 24.

The Eu anomaly is commonly explained by shallow crystal fractionation within the evolving magma especially the extraction of plagioclase. The Eu anomaly has also been compared to the Ce/Yb ratio. Ce and Yb are both incompatible in plagioclase, however Yb is even more incompatible then Ce so plagioclase fractionation on residual melt would have a twofold effect: create a negative Eu anomaly, and decrease the Ce/Yb ratio (Zullo, 1991). This is shown in figure 25-A.

The least fractionated, with smaller negative Eu anomaly and Ce/Yb ratio, are the syenites (562110, 562116, and 562123) these are generally the assumed host rocks (L0, L1, L2 and L9) unassociated with pegmatites/ microsyenites and showing little of the biotite alteration in thin section. These syenites (red in figure 25-A) show the magmatic evolution of the outcrop, with progressive fractionation of plagioclase they form a linear correlation of reducing Eu/Eu* and Ce/Yb (red line figure 25-A, Ce/Yb: from 55 to 25 and Eu/Eu*: from 0.6 to 0.25) which has an excellent correlation with an R^2 ratio of 0.97. This is indicative of an evolving magmatic source with progressive fractional crystallization. The microsyenites and pegmatites on the other hand appear to have been derived from an already evolved magmatic source with a consistent Eu/Eu* and Ce/Yb ratios of ~0.25 and ~25 respectively. They correlate with the highest fractionated syenite samples indicating they have gone through similar degrees of fractionation. The microsyenites also appear to have a small correlation with a similar degree of fractional crystallization (Eu/Eu* ~ 0.25) while the variation in Ce/Yb ratio indicates various levels of plagioclase extraction (from 38 to 22).

The same data has are plotted with TREE+Y+Nb+Zr+Ta in ppm (figure 25-B).Here the samples split into two clearly defined groups, those mineralized (green box) consisting of pegmatites and one microsyenite with a NTZR value from 10,500 to 20,000 ppm and an Eu/Eu* value of 0.25 and those not mineralized (red box) consisting of syenites with low mineralization 100- 5000 ppm NTZR value and a Eu/Eu* value of 0.6-0.25. The fact that there is both mineralized and unmineralized samples with a low Eu/Eu* value means that the fractionation was not the driving mechanism behind the mineralisation.

Figure 25-B also shows that the syenites have increasing negative Eu anomaly that correlates with a slight increasing trace and REE concentrations. This is the limit of NTZT concentration via fractional crystallization. The Eu/Eu* ratio for all samples does not fall below ~0.25 and is the outcrops highest degree of fractional crystallization. It is at this value where the highest concentration of NTZR occurs. The pegmatites, the syenites from L8 (which was layered and associated with pegmatites) and the microsyenites all have roughly the same Eu anomaly with varying

amounts of NTZR concentrations. Hence, fractionated late stage magma must have played some part in the mineralization process.

The split seen in mineralized an unmineralized samples is highlighted when plotted against Tot/C (figure 25-C), the mineralized samples in the green box have distinctly more carbon with a Tot/C value of 0.25-0.3 wt% than those of the unmineralized samples (blue box) ~0.02 wt%. This clearly shows that the fractionated samples need the input of carbon in order to develop NTZR mineralization. Not displayed in figure 25 is with the addition of increased carbon potentially CO_2 there is also a significant increase in the elements of U, Sn and Hf within these samples.

Figure 25-D and E try to differentiate the REE based upon their geochemical characteristics. The REE can be split into two distinct groups: the light (LREE La-Eu) and heavy REE (HREE Gd-Lu+Y) which is physically based upon their ionic radius. This variation in ionic radius plus a unique aspect to the REE "lanthanide contraction" (their ionic size decreases with the increasing ionic number (Douglas, 1954)) causes slight changes in chemical and fractionation behavior relative to each other. The concentration of HREE compared to the LREE is important economically which is discussed later in this thesis. The ratio of LREE to HREE has been calculated and when compared to the Eu/Eu* ratio the fractionation behavior seen in the syenites is again apparent and they simultaneously have developed a greater HREE signature. The development of this HREE signature is intimately related to fractionation. The greater fractionation as seen in Figure 25-D the greater development of a HREE signature. Peralkaline REE deposits associated with pegmatites often have this HREE signature as is seen in other deposits similar to the MAMC. Figure 25-E shows that the HREE signature is associated with a drop in P_2O_5. This correlation is also seen in the major elements TiO_2 and MgO. There is no positive correlation with the development of a HREE signature with the major elements however the trace elements Be, Ga, Hf, Rb and Sn do increase whose incompatible nature has developed concentrations through the fractional crystallization.

The size of the point in figure 25-E shows the NTZR concentration in ppm. It shows that the mineralization concentration is not specifically linked with the fractionation or the development of a HREE signature as there are some samples with these signatures that do not have higher concentrations of NTZR.

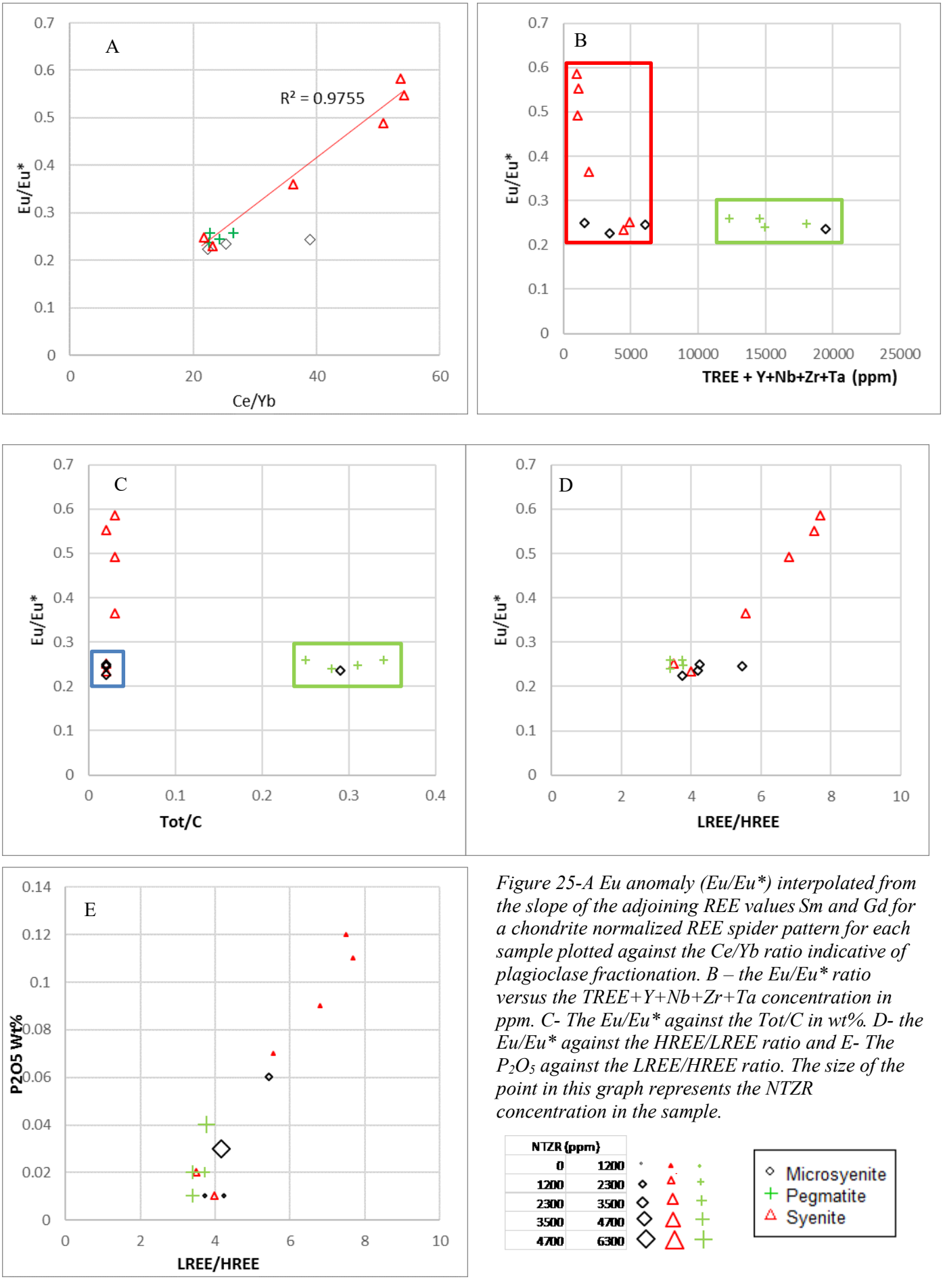

Figure 25-A Eu anomaly (Eu/Eu) interpolated from the slope of the adjoining REE values Sm and Gd for a chondrite normalized REE spider pattern for each sample plotted against the Ce/Yb ratio indicative of plagioclase fractionation. B – the Eu/Eu* ratio versus the TREE+Y+Nb+Zr+Ta concentration in ppm. C- The Eu/Eu* against the Tot/C in wt%. D- the Eu/Eu* against the HREE/LREE ratio and E- The P_2O_5 against the LREE/HREE ratio. The size of the point in this graph represents the NTZR concentration in the sample.*

8. Discussion on outcrop scale investigations.

8.1 Petrological relationships.

The outcrop samples from the Stoorelv location can be divided into three rock types: syenites, microsyenites and pegmatites. These three can be distinguished by their petrography and show distinctive features in trace element geochemistry. Their similarity in the major element geochemistry (figure 23) does indicate a similarity in the major element composition of the source of the different rocks of the outcrop. The pegmatites show most variation in their composition and their variation in SiO_2 gives them a major geochemical signal similar to that of the MSF. The rest of the samples plot similarly to both the GF and MSF samples.

The main mineral components of the syenites are: nepheline, and k-feldspar, and mafic 'clots' of amphibole, biotite and clinopyroxene. There are no REE hosting minerals identified and very little alteration. In the outcrop these syenite units are fully encompassed by microsyenites and pegmatites creating vast (10's of m) syenite rafts. The microsyenites, when sampled from the inner sections of the layer, are similar in trace element composition to the syenites except finer grained (1-2mm). When taken closer to the contact with the syenites, or pegmatites the trace element composition changes. Amphiboles in these samples have often been replaced with biotite and there is a high abundance of minerals such as hematite, pyrochlore and trace zircon which are often found in clusters. Similarities also exist in the contact pegmatites which have an intimate stratigraphic relationship to the microsyenites. These pegmatite samples contain of REE bearing minerals including pyrochlore (Figure 20 and Figure 21), zircon, thorite, eudialyte and bastnäsite.

Stratigraphically the coarse grained syenites (Table 2 and figure 13) are the least evolved, best represented by samples 56210, 562116 and 562118. They have the lowest NTZR concentrations and are the least fractionated. These three samples are less fractionated versions of the other syenite samples in the outcrop (562121 and 562122) which shows a magmatic evolution of the syenite samples and a magmatic fractionation trend in the Eu/Eu* in this outcrop.

The microsyenites and the pegmatites all have similar Eu/Eu* fractionation ratios, higher than those of the coarse grained syenites and appear as one group in figure 25. The fractionation trend for the syenites relate to the evolution of the GF as one source, while the consistent Eu/Eu* ratio, major geochemistry and the stratigraphic relationships of the microsyenites and the pegmatites indicate that these could be different a second source. The three groups of samples seen in this dataset (Figure 25- blue, green and red box) could show this. Late stage magmatic fluids of the MSF enriched in trace elements through fractionation may provide an explanation for the development of microsyenites and further enrichment through fluid flow may be the cause for the pegmatites intruding into the GF syenites.

The pegmatites have been suggested to form according to the Jahns and Burnham model (Thomas et al, 1988) forming from a late stage magmatic fluid. One possible source for this could be the microsyenites. This relationship is seen petrographically and geochemically with the pegmatites having an intimate relationship with the microsyenite units only forming at its contacts and with the similar level of fractionation highlighted in the groupings in Figure 25. Noted

in the field were fragmented microsyenite contacts seen in the outcrop which were filled with pegmatite and are indicative of the magma being fragmented during the release of volatiles during degassing (Thomas et al, 1988).

This formation of pegmatites from late stage magmatic fluids potentially through degassing of the microsyenites could be a source of the trace element enrichment. By mobilizing trace elements from the microsyenites into highly concentrated fluids which then form the enriched pegmatites at boundaries of microsyenites explains the enrichment seen. This even extends to where pegmatites haven't formed but element enrichment has (see sample 562117). This sample is taken directly from a fragmented boundary between the syenite and the microsyenite. This indicates that mineralization was occurring at layer boundaries even when pegmatites did not from possibly exploiting zones of weakness and precipitating NTZR minerals into the cooling contact zones.

The NTZR element concentrations and the fractionation ratios of these samples as well as the stratigraphic relations indicate that late stage microsyenites enriched in trace elements through fractionation intruded into the less fractionated syenites. While cooling the microsyenites formed a very late stage enriched aqueous fluid which degassed while the microsyenites formed. This degassing fragmented the cooling microsyenite magma forming broken contacts and precipitating pegmatites at the boundaries and it was within these that the REE hosting minerals precipitated.

8.2 Controls on Nb-Ta-Zr-REE (NTZR) mineralization.

The main concentrations of Nb-Ta-Zr-REE lie in the pegmatites and one contact microsyenite (figure 24). The partitioning between the rock samples can be explained by the trend in magmatic evolution and late stage magmatic fluid interactions. This is best seen in figure 25, some fractionated samples are the ones that are most enriched in Nb-Ta-Zr-REE but further processes were important to raise the trace element concentrations as it is not ubiquitous.

The more peralkaline samples concentration were further enriched in incompatible trace elements through fractional crystallization. As the melt evolved, it underwent fractional crystallization, this process caused the incompatible trace elements to be concentrated into smaller melt volumes. These late stage melts are represented by the peralkaline microsyenite samples. These microsyenites formed through prolonged fractional crystallization which is shown by their increased Eu anomaly and contained elevated concentrations of incompatible elements (figure 25 and figure 26).

The secondary process that occurred involved CO_2 as all the highly mineralized samples have elevated Tot/C %. The pegmatites at the contacts of the microsyenites crystalized from highly enriched magmatic fluids potentially derived from the evolved microsyenites. The mobilization of the trace elements into these fluids could be due to the inclusion of volatiles which aided in mobilization of the trace elements. These volatiles could have been derived from an external source which further aided in enriching the fluids circulating through the crystal mush redistributing the elements into the fluids and finally precipitating in the pegmatites. The precise role of CO_2 in this process is unclear but it has been suggested that it could aid in precipitating the trace elements from solution, the Cl and F concentrations in these samples show no correlation so there must have been other mechanisms involved in mobilizing these trace elements. But it is clear that Tot/C% is distinctly related to the mineralization. A possible source for these elements may

come from the overlying the reworked Archaean terranes of the Eriksfjord formation; which consists of: quartzites, basalts trachytes.

A positive correlation with fractionation and development of a HREE signature is also seen. This is common among pegmatite REE deposits as the late stage magmatic to hydrothermal processes that concentrate the REE can aid in the precipitation of HREE bearing minerals. There is a negative correlation of some major elements with this development of a HREE signature. Al-Ani & Sarapää, (2009) observed a positive relation between LREEs and P_2O_5. Conversely the development of a HREE signature in these samples caused the Wt% of P_2O_5 to become diluted in the samples due to the addition of elements related to increasing HREE signature such as the HREE mineralization and other elements such as: Be, Ga, Hf, Rb and Sn.

Comparison of the Nb-Zr-Ta and the TREE concentrations of the regional and local dataset is shown in figure 26. It shows a very positive correlation between Nb-Zr and Ta and TREE, in the peralkaline syenites regionally, and in the pegmatites and microsyenites locally. The Nb-Zr-Ta and REE behave similarly when entering or precipitating from the fluid phase. Increasing crystallization and precipitation of minerals that contain rare earth elements often also incorporate Nb-Zr and Ta such, as zircon. So, while conditions favored the precipitation of REE bearing minerals, the conditions were also favorable to Nb-Zr and Ta, concentrations usually in the same minerals. Additionally, the strong correlation seen in the outcrop samples of the syenite and microsyenites is indicative of magmatic differentiation and development of the evolving magma. The disassociation of observed NTZR ppm between the highest enriched regional samples and outcrop samples is due to the changing methods of sampling and the number of elements tested.

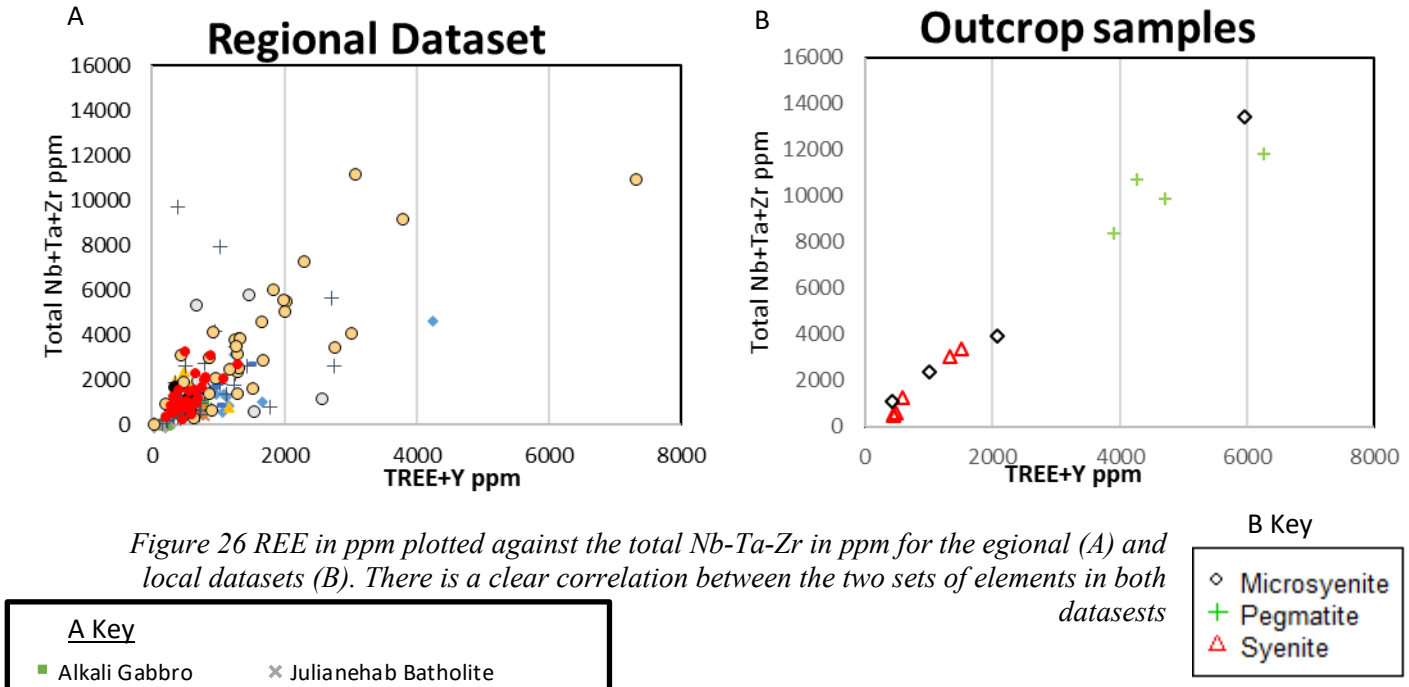

Figure 26 REE in ppm plotted against the total Nb-Ta-Zr in ppm for the egional (A) and local datasets (B). There is a clear correlation between the two sets of elements in both datasests

9. Conclusions and further questions.

9.1 Regional scale

The MAMC shows a regional trend in normative mineralogy of syenite rock units evolving from the oldest quartz dominated GF (ranging from quartz-monzonite to foid-bearing monzonite) through the middle highly variable MSF (ranging from silica saturated monzo-granite to foid-monzosyenite) to the youngest silica undersaturated FDF (ranging from foid-bearing monzonite to foidolite). The oldest and middle formations the GF and MSF respectively have a major geochemical signatures that been enriched in trace elements via the addition of large scale circulation of fluids and incorporation of country rock, as seen in Figure 9. These interactions have caused an elevated silica saturation in MSF and GF samples.

A combination of crystal fractionation enriching trace elements and the addition of volatiles potentially associated with assimilation of country rock aided in mobilization and concentration of NTZR elements. Precipitation of trace element rich minerals in late stage peralkaline microsyenite units caused these rocks to be significantly more enriched than other syenites in the area.

The peralkaline microsyenites have elevated concentrations of NTZR trace elements due to their peralkalinity and the high degree fractionation. Potentially the incorporation of country rock along the outer edges of the MAMC provided volatiles which enabled the NTZR mobilization through circulating fluids which further enriching the Nb-Zr-Ta-REE concentrations.

The younger FDF intruded into the core of the MSF and was therefore sheltered by the older unit from any fluid circulation or country rock interactions. Hence it maintained its original composition and further enrichment of the trace elements concentrations (Figure 3 and figure 9).

9.2 Local scale

The syenites, microsyenites and pegmatites from the outcrop in the Stoorelv valley are located in the GF formation. They can be distinctly differentiated by their trace element distributions. The syenite samples show a clear magmatic fractionation trend, the most fractionated samples also include the microsyenites and the pegmatites potentially derived from MSF magma. In general, the more fractionated the sample the more they develop a HREE signature but does not significantly increase NTZR concentrations. Significant concentrations of NTZR lie only in the pegmatites and at microsyenites found in contacts. The process of precipitation of these is thought to include very late stage orthomagmatic volatile rich fluids enriched in NTZR moving through the highly fractionated microsyenites. Aided by volatiles such as CO_2 from external sources caused the remobilization and further concentration of NTZR mineralization into these fluids, which eventually degassed from the microsyenites at contacts and precipitated enriched pegmatites. The degassing of volatile rich fluids from the microsyenites caused the fracturing of contacts at the microsyenite layer boundaries and precipitated trace element rich pegmatites.

This processes allowed a fluid to form that aided rare elements that could incorporate incompatible elements into their crystal lattice. Rare minerals with elevated concentrations of Nb-Ta-Zr-REE include: pyrochlore, zircon, thorite, eudialyte and bastnäsite which can be found in the pegmatites and microsyenite samples. The presence of heightened Zr concentrations is also thought to aid in the formation of these minerals. The recrystallization of quartz at grain boundaries in some of the more enriched samples indicate that some fluids were flowing through the crystal mush (Figure 22) and this is the proposed late stage process that could further remobilize and concentrate these incompatible elements into the pegmatites layer contacts.

The similarity in Eu/Eu* anomaly of the microsyenites and the pegmatites suggests a similar source for microsyenites and pegmatites. Additionally, this similarity could suggest that these samples are also derived from a different source to that of the syenites. The providence of the microsyenites and pegmatites is not conclusive since they are so similar in geochemical and perographical characteristics between the GF and the MSF. However, stratigraphic relationships suggest the late stage peralkaline magmatism of the MSF as the likely source.

9.3 Further questions

During this investigation several questions have arisen that can lead to further work:

1) Does the fractionation of the pegmatites and microsyenites in outcrop represent the highest amount of fractionation in this intrusion, or is this outcrop representative of the latest stage of magma fractionation? Does this vary spatially? Were there greater amounts of fractionation elsewhere and therefore is there greater concentrations of NTZR minerals derived from this magmatic process elsewhere in the MAMC?
2) A greater focus on the providence of the microsyenites, where was the microsyenites and pegmatites derived from, is it external from the MSM or locally sourced from the GF?
3) Greater confidence that the pegmatites and microsyenites are related, or are they separate?
4) What is the source of the CO_2, and did it aid in mobilizing the NTZR mineralization, did it aid in precipitating the NTZR mineralization, or neither, as it could be parallel to the mineralization? What other key volatiles were important in enriching the NTZR mineralization in the pegmatites?

9.4 Economic potential of the Motzfeldt REE mineralization.

The market for REE is controlled by two key factors, availability and demand. The demand for REE is growing due to their importance in the new technologies and the growing 'green' technology market. However, the availability of these elements is decreaing at this time due to inconsistencies in production from a mainly Chinese dominated market. Also, the availability of economic concentrations of LREE or HREE does vary depending on the deposit type mostly favoring LREE concentrations due to the HREE being slightly more compatible with the mantle. The MAMC is of interest as REE are growing in demand and it is a potential deposit located outside of China. Also, it may hold economic concentrations of heavy rare earth elements and therefore worth exploration.

The REE market today is dominated by Chinese supply, 97% of the world's supply of REEs comes from Chinese sources. Of this, 40-50% total production comes from only one deposit: the carbonatite Fe–REE–Nb deposit at Bayan

Obo mine at Inner Mongolia (Chankhmouradian & Zaitsev, 2012 and Zhang et al., 2017). China's REE production is so overwhelming on the world market that the demand for a European producing deposit to relieve Chinese reliance is a priority. The potential to have a REE source in Greenland could help relieve some of this market imbalance.

REE deposits associated with pegmatites and alkaline intrusions usually have an association with comparatively high HREE abundances while carbonatites are usually associated with LREE enrichment. The majority of REE production comes from carbonatites and has caused an imbalance in the abundance of LREE and HREE in the market. The HREE are significantly less abundant than LREE, so much so that some of the HREE are classed as critical as their use outstrips supply. The explosion of green technologies which is heavily reliant on HREE has caused a demand increase for these elements. The potential that the alkaline MAMC could host a HREE enriched deposit makes it also of great interest (Stine, 2014 and Henderson, 2011).

The REE concentrations in the samples derived from the MAMC have been geochemically compared to 50 other known REE deposits from outside china (including: Africa, Australia, Brazil, Canada, Germany, Greenland, Kazakhstan, Sweden, Turkey, and the USA) to see how they compare to other world resources. Data for this was taken from Paulick & Machacek (2017), Kalashnikov (2016) and Sørensen (2003). In figure 27, average reserve values of 50 deposits have been plotted showing the TRO (Wt%) vs the ratio of LREE/HREE. The outcrop samples have been converted to TREO Wt% and plotted alongside the world data. The world deposits have been split by deposit type: silicate – dominated deposits, phosphate- dominated deposits and carbonate – dominated deposits.

The clear majority of the known deposits lie in the LREE dominated upper half of the diagram, there a few deposits with significant HREE concentrations (mainly phosphate dominated) with most having a LREE/HREE ratio of 0.8-0.99. There is a slight relationship with an increasing HREE signature correlating with a lower TREO. Which shows how the supply of HREE is limited.

Deposits range in TREO from 0.3-14 Wt% most LREE dominated deposits have above 1 Wt% TREO. The carbonates hold the majority of the LREE dominated deposits and, on average, have higher TREO concentrations. Phosphate and silicate deposits generally have lower LREE to HREE ratios with phosphates having the potential to form greater TREO concentrations. Importantly the HREE deposits show a vast reduction in the TREO concentration which is seen globally as LREE deposits in economic concentrations are much more common. Most of the HREE deposits lie with a TREO 0.1-1 Wt% and a LREE/HREE of 0.2-0.8.

The samples of the regional study (red, black and green) lie lower in the LREE/HREE ratio (0.8) than those of the high TREO carbonate and phosphate deposits (0.9). Also the outcrop samples have an average TREO Wt% compared to a deposit with a HREE signature (0.9 Wt%). When compared to other HREE signature deposits they are not especially enriched in HREE compared to that of other deposits of similar TREO. While other deposits of similar concentrations have a LREE/HREE of 0.65 the outcrop samples lie in the upper quartile of this ratio. The syenites (red) lie in the region found with other low concentration deposits but are not comparatively enriched in HREE. The most enriched microsyenite and pegmatites lie in the same region as other moderately enriched deposits.

This could indicate that the MAMC doesn't have much potential to be an important REE resource as it has a moderate TREO Wt% and relatively high LREE/HREE signature. It does have similar TREO Wt% to other deposits: 1%, but it does not have a particularly high HREE signature. This means it is not particularly unique or outstanding. However, it being outside China, and with the development and presence of other deposits being explored in the Grader province providing interest in the area it could make this a resource still of some interest for further exploration. The infrastructure and investments in surrounding deposits, linked with the political and mining stability of Greenland could make this more inviting for potential investment and exploration.

It must be noted as well that the data could be slightly misleading as the samples are so selective. The thin (20 cm) and discontinous nature of the pegmatites mean they could be unrepresentative of the entire MAMC. The syenite samples could be seen as a more representative of the MAMC and GF as a whole. The pegmatite sheets for example could be volumetrically insignificant or discontinuous making them and their mineralization irrelevant to mining or show an increase in TREE Wt% or reduction in HREE/LREE ratio in other areas of the MAMC. The nature of the syenites throughout the MAMC needs to be better understood and the extent and volume of these pegmatites and microsyenites within the MAMC outlined. Preliminarily the samples represent an interesting observation and could provoke further exploration/drilling to understand the extent and nature of the pegmatites within the MAMC.

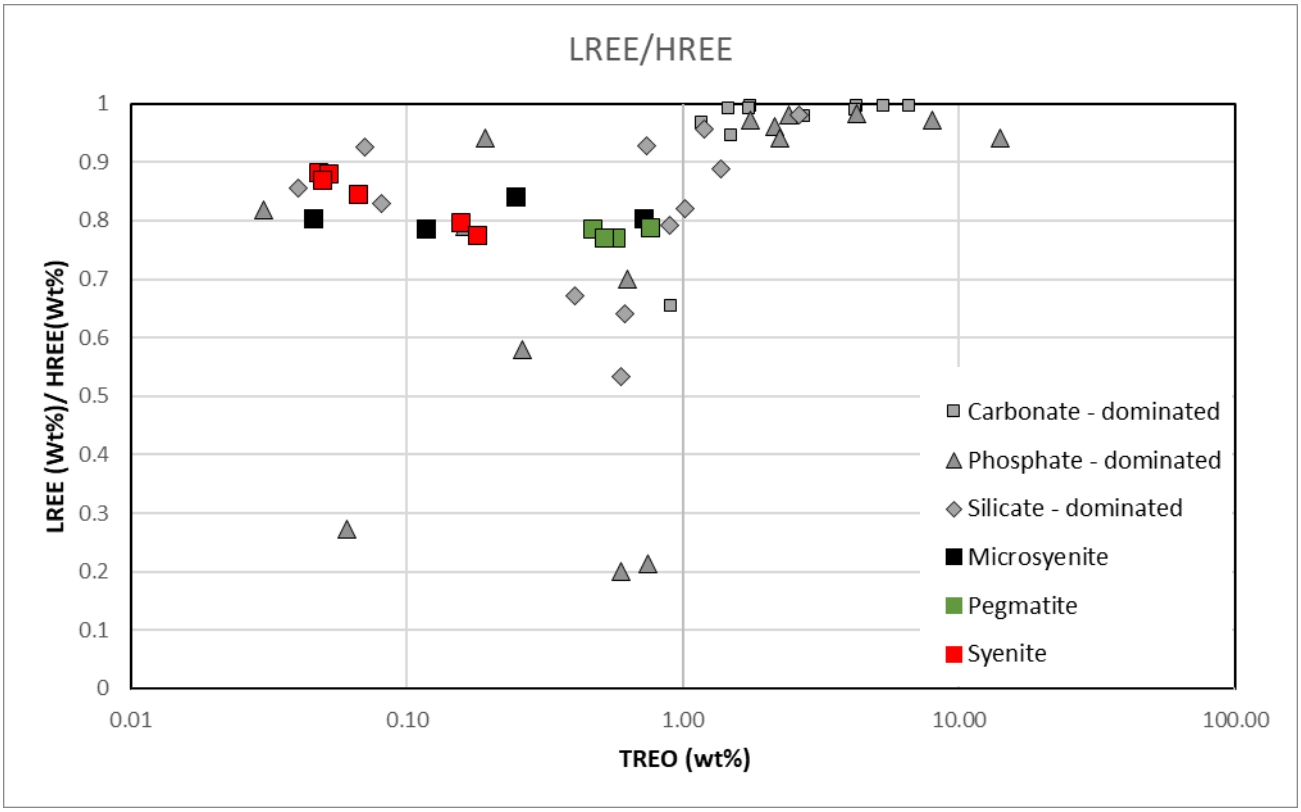

Figure 27 TREE in ppm against the LREE/HREE ratio for the regional samples (Square: black; microsyenite, green; pegmatite and red; syenite) and other deposits outside of China (grey: square; carbonate – dominated, triangle; phosphate- dominated and diamond; silicate – dominated deposits. The upper half of the diagram shows those deposits more enriched in LREE than HREE while the lower half are those enriched in HREE compared to LREE. They have been plotted against the TREO concentrations in ppm for the elements La, Ce, Pr, Nd, Sm, Eu, Gd, Tb, Dy, Ho, Er, Tm, Yb, Lu and Y in ppm. Data for this was taken from Paulick & Machacek, (2017), Kalashnikov, (2016) and Sørensen, (2003).

10. BIBLIOGRAPHY

Al-Ani T, & Sarapää O (2009). Geochemistry and Mineralogy of REE in Virtasalmi kaolin deposits, SE Finland. Rovaniemi: GTK.

Blaxland A, Breemen O, Emeleus C, Anderson J (1978). Age and origin of the major syenite centres in the Gardar province of south Greenland: Rb-Sr studies. Geological Society of America Bulletin, 231-244.

Bradshaw C (1988). A Petrographic, Structural and Geochemical study of the alkaline igneous rocks of the Motzfeldt centre, south Greenland. University of Durham: The Graduate Society.

Brumme A (2014). Market analysis of rare earth elements. In A. Brumme, Wind Energy Deployment and the Relevance of Rare Earths, pp. 17-48.

Chankhmouradian AR, Zaitsev NA (2012). Rare Earth Mineralisation in Igneous Rocks: Sources and Processes. Elements, 347-353.

Cox K, Bell J (1979). Trace elements in igneous processes. In The interpretation of igneous rocks, Great Britain: The University press, pp. 332-360.

Douglas E (1954). The Lanthanide contraction. Pittsburgh: The University of Pittsburgh, 1-4.

Finch A, Goodenough K, Salmon H, Anderson T (2001). The petrology and petrogenesis of the north Motzfeldt Centre, Gardar Province, South Greenland. Mineralogical Magazine, 759-774.

Garde A, Chadwick B, Grocott J, Swager C (1996). Metasedimentary rocks, intrusions and deformation history in the south-east part of the c. 1800 Ma Ketilidian orogen, South Greenland. Copenhagen: Geology of Greenland Survey Bulletin. 1-5

Gill R (2010). Alkali Rocks. In Igneous rocks and processes a practical guide. London: Wiley-Blackwell, pp. 291-345.

Henderson P (2011). Rare Earth Elements. Geological Society of London. 1-5.

Jones AP (1984). Mafic silicates from the nepheline syenites of the Motzfeldt centre, South Greenland. Mineralogical Magazine, 1-12.

Le Bas MJ (1986). A chemical classification of volcanic rocks based on the total alkali-silica diagram. Journal of Petroleum Science and Engineering, 745-750.

Kalashnikov A (2016). Rare earth deposits of the Murmansk region, Russia - A Review. Society of Economic Geologists, 111, 1529-1559.

MacDonald R, & Upton, B. G (1993). The Proterozoic Gardar rift zone, south Greenland: comparisons with the East African Rift System. Geological Society, London, Special Publications, 427-442.

McCreath JA, Finch AA, Simonsen SL., Donaldson CH, Armour-Brown, A. (2012), Independent ages of magmatic and hydrothermal activity in alkaline igneous rocks: The Motzfeldt Centre, Gardar Province, South Greenland, Contributions to Mineralogy and Petrology, 163: 967.

Paulick H, Machacek E (2017), The global rare earth exploration boom: An analysis of resources outside of China and discussion of development perspectives, Resources Policy, 134-153.

Rolland Y, Cox S, Boullier AM, Pennacchioni G, Mancktelow N (2003). Rare earth and trace element mobility in mid-crustal shear zones: insights from the Mont Blanc Massif (Western Alps), Earth and Planetary Science Letters, Volume 214, Issues 1–2, 203-219.

Stine EL (2014). Heavy Rare Earth Elements (HREE) opportunities in Queensland. Queensland: Department of Natural Resources and Mines.

Sørensen H (2003). Development of Nepheline Syenites in rift zones – Information from three Rift complexes. GeoLines, 140-146.

Streckeisen A (1974). Classification and nomenclature of plutonic rocks recommendations of the IUGS sub commission on the systematics of Igneous Rocks. International Journal of Earth Sciences, 773–786.

Thomas VA, Bray JC, Spooner TE (1988). A discussion of the Jahns–Burnham proposal for the formation of zoned granitic pegmatites using solid-liquid-vapour inclusions from the Tanco Pegmatite, S.E. Manitoba, Canada. Earth and Environmental Science Transactions of the Royal Society of Edinburgh, 2-3.

Tukiainen T (2014). The Motzfeldt of the Igaliko nepheline syenite complex, south Greenland – a major resource of REE elements. Copenhagen: 1st European Rare Earth Resources Conference.

Upton BG (1978). The Gardar Igneous Province: evidence for Proterozoic continental rifting. Petrology and Geochemistry of Continental Rifts, 163-172.

Upton BG (2013). Tectono-magmatic evolution of the younger Gardar southern rift, South Greenland. Copenhagen: Geological Survey of Denmark and Greenland.

Upton BG, Emeleus CH, Heaman LM, Goodenough KM, Finch AA (2003). Magmatism of the mid-Proterozoic Gardar province, South Greenland: chronology, petrogenesis and geological setting. Lithos, 43-65.

Upton BG, Parsons I, Emeleus CH, Hodson ME (1996). Layered alkaline igneous rocks of the Gardar province, South Greenland. Developments in Petrology, 331-363.

Voncken JH (2013). Applications of the rare earths. Rare Earth Elements an Introduction, pp 89-103.

Walters A, Lusty P (2011). Rare earth Elements. London: BSGS, Centre for sustainable mineral development.

Zhang SH, Zhao Y, Yongsheng L (2017). A precise zircon Th-Pb age of carbonatite sills from the world's largest Bayan Obo deposit: implications for timing and genesis of REE-Nb mineralization. Precambrian Research, 1-58.

Weatherley S (2016). Motzfeldt 2016 Field Diary. Copenhagen: GEUS.

Zullo JW (1991). Geology Of Carolinas: Carolina Geological Society 50Th Anniversary Volume (1 ed.). Carolina.